

**Mesoporous g-C₃N₄ Decorated with Cu Nanoparticles for
Enhanced Photo-Degradation for Tartrazine Yellow**

JIAHE XU

A thesis submitted to the
School of Graduate Studies
Rutgers, the State University of New Jersey

In partial fulfillment of the requirements

For the degree of

Master of Science

Graduate program in Chemical and Biochemical Engineering

Written under the direction of

Tewodros Asefa

And approved by

New Brunswick, New Jersey

October 2018

ABSTRACT OF THE THESIS

Mesoporous g-C₃N₄ Decorated with Cu Nanoparticles for
Enhanced Photo-Degradation for Tartrazine Yellow

By: JIAHE XU

Thesis Director:

Prof. Tewodros Asefa

Two strategies were combined to modify the carbon nitride, which are creating a mesoporous structure, and deposition of Cu nanoparticles, to create high specific surface area within a carbon nitride framework and inhibit the recombination of electron and hole pairs, thereby increase the efficiency of photocatalytic activity. To make the material, melamine powder, which is inexpensive, easy to get and non-poisonous, was used as precursor and, SiO₂ was used as a hard template to create a different size mesoporous structure through a simple thermal condensation method. Two different desired amount of copper nanoparticles were deposited on the surface of mesoporous carbon nitride (MCN) which are 5% and 10% wt.% through a simple precipitation-reduction method. To further investigate the photocatalytic activity, the Cu-MCN materials were used as photocatalysts for degradation of tartrazine yellow which is a harmful dye in aqueous solution under UV-light irradiation. The result showed that Cu-MCN has good photocatalytic activity under light irradiation. Among six samples synthesized, Cu(10)-MCN showed the best photocatalytic activity due to its mesoporous structure and optimized amount and type of Cu in it. A mechanism was proposed to explain the effectiveness of material to photo-degrade tartrazine yellow.

Finally, we make some suggestion which highlighted the future development of g-C₃N₄ based photocatalysts.

Dedication

Dedicate to my parents

and beloved Rabbit

without whom this thesis would be never completed

Acknowledgement

Firstly, I would like to thank my adviser Prof. Tewodros Asefa for his patience and selfless guidance. He never pushes me, but always provides me with the best advice. The experience being a master student of Prof. Tewodros Asefa is a great honor. The research experience in lab has made me grown-up. I would also like to thank Prof. Charles Roth and Prof. Nina Shapley for being members of my committee

Secondly, I appreciate the friendship and help from my lab colleagues Tao Zhang, who is currently a PhD student in Asefa's group. He is such a nice person. He taught me a lot about scientific research, and always share his opinion with me.

I also would like thank our Brazilian friend, Prof. Vitor C. Almeida, as well as his students for their help with instruments analyzing the samples that I have synthesized during my research work.

In addition, I would like to thank my best friend Han Cao. Life in another country will be tough and lonely. The most enjoyable time is to chat with him on the phone. His accompany helped me overcome obstacles and be able to finish two years master study at Rutgers University.

I would like to thank my friend XiaoHan Zhang for his help with drawing figures and advice during writing my thesis.

Finally, I must thank the Almighty God for his protection for me to be here in the United States of America.

Table of Contents

Abstract of the thesis	ii
Dedication	iv
Acknowledgement.....	v
Abbreviations	vii
List of figures	viii
List of tables.....	x
1. Introduction.....	1
1.1 The photochemical conversion and storage of solar energy.....	1
1.2 The semiconductor photocatalyst	7
1.3 Introduction of graphitic carbon nitride.....	13
1.4 Introduction of tartrazine yellow	18
2. Experiment procedure	21
3. Characterization	25
4. Photocatalytic activity procedure.....	26
5. Result and discussion	28
5.1 Transmission electron microscopy (TEM) analysis	28
5.2 X-Ray diffraction (XRD) pattern	31
5.3 Thermogravimetric analyses (TGA) of the materials.....	33
5.4 The specific surface area and pore size distribution.....	35
5.5 Photocatalytic activity	38
5.6 Possible photocatalytic mechanism	43
6. Conclusions.....	47
7. References	49

Abbreviations

°C	Degree Celsius
%	percent
MCN	mesoporous carbon nitride
Cu-MCN	copper doped mesoporous carbon nitride
nm	nanometer
cm	centimeter
mL	mili liter
h	hour
g	gram
M	molar per liter
mg	mili gram
min	minute
C_t	tartrazine yellow concentration in solution at time t
C_0	the original concentration of tartrazine yellow
TEM	transmission electron microscopy
N_2	nitrogen
O_2	oxygen
H_2O	water
e^-	electron
h^+	hole
Cu	copper

List of Figures

Figure 1. (a) Oil discovery trend and (b) world production of oil.....	3
Figure 2. Three types of energy conversion from solar energy: electricity, fuel, heat	5
Figure 3. Primary steps in the photoelectrochemical mechanism	9
Figure 4. The chemical structure for C_3N_4 (a) trizine and (b) tri-s-trizine.....	14
Figure 5. Schematic illustration of the main routes for the synthesis of g- C_3N_4	15
Figure 6. The molecular formula of tartrazine yellow and real object of tartrazine yellow.....	18
Figure 7. The mixture of C_3N_4 and SiO_2	21
Figure 8. Ground the mixture into powder.....	21
Figure 9. Removal of SiO_2 by NH_4HF_2	22
Figure 10. Filtering the suspension.....	22
Figure 11. The sample of mesoporous carbon nitride	22
Figure 12. The sample of Cu- C_3N_4 and m- C_3N_4	23
Figure 13. (a) Transmission electron microscopy (TEM) image of 22 nm m- C_3N_4 (b) Transmission electron microscopy (TEM) image of 22 nm Cu(10)-m- C_3N_4 (c) Transmission electron microscopy (TEM) image of 47nm Cu(10)- m- C_3N_4	27-28
Figure 14. XRD pattern of synthesized sample.....	30
Figure 15. TGA plot of material.....	32
Figure 16. (a) N_2 adsorption–desorption isotherms and (b) pore size distributions of MCN, Cu(5)/MCN and Cu(10) MCN.....	34

Figure 17. (a) The photocatalytic degradation of tartrazine yellow under light irradiation over bulk CN, 22 nm MCN, 47 nm MCN, 22 nm Cu(5)MCN, 22 nm Cu(10)MCN, 47 nm Cu(5)MCN and 47nm Cu(10) MCN photocatalysts and, (b) (c) (d) Time-dependent UV–vis absorption spectra for the catalytic degradation of tartrazine yellow over the 22 nm MCN, 22 nm Cu(5) MCN, 22 nm Cu(10) MCN photocatalyst.....37-38

Figure 18. Mechanism of photocatalytic degradation of dye solution over the Cu/MCN photocatalyst.....44

Figure 19. (a) The trapping experiment and (b) The Mott–Schottky plot for the MCN sample.....44

Figure 20. Detailed possible mechanism of photo-degradation of tartrazine yellow by Cu/MCN.....47

List of Tables

Table 1. The surface area of synthesized sample.....	35
Table 2. The mass of each sample.....	39
Table 3. The photodegradation rate for 240 min over 6 sample under the irradiation of UV light.....	39

1. Introduction

1.1 The photochemical conversion and storage of solar energy

Through the ages, human never stop pursuing energy. In the day we discovered fire, civilization has begun. Mankind has had a history of 4 million years so far. During this period, mankind began to learn to use fire, passed through the ages of stone and iron tools, and reached modern industrial revolution. Various technological inventions have brought human civilization to an unprecedented height. At the same time, the energy consumed by humans has also been growing. Among them, coal and petroleum are the major sources of energy today.^[1] Energy is the basic material for the survival and development of human society, and it has a particularly important strategic position in a country's national economy. Energy is also like a "city's blood", and drives the city's operation. However, the petroleum and biomass are not infinite. How long can oil last on the earth and be used by humans? Although this may not be precisely known, many experts believe that the oil on Earth can last only thirty or forty years, and some experts believe that it can be used for one to two hundred years.^{[1] [2]} On June 7, 1998, the "Los Angeles Times" in the US published an article entitled "The Coming Oil Crisis - The Real Crisis" that in the next 10 years or so, the world's oil supply seems to be sufficient. In the next 20 years or so, global oil production may begin to decline continuously. Although improvements in market forces and oil production technologies may keep oil supply up until the 21st century, the arrival of the oil crisis may be much earlier than most people think. At present, the world's daily consumption of oil has reached 71 million barrels, an increase of almost 2% per year.^{[3] [6]} On the basis of this annual increase, by 2010, the world will consume half of all oil in the earth.^[3] Despite

the dramatic advances in geological exploration technology, the oil reserves proved to be significantly reduced because the ratio of existing oil consumption to newly discovered oil is 4:1.^[4] By 2003, both developed and developing countries would eventually face the oil crisis. In this century, the world is relying on energy-dense, low-priced oil to push its economy forward. If the oil is depleted, the world economy will face severe challenges. Some scientist believed that by the end of 1997, oil extraction had reached 807 billion barrels, half of which was mined in the oil turmoil of 1970s.^[6] ^[7] According to some conservative estimates, oil reserves will not exceed 830 billion barrels.^[4] There are also some reports that the world's total oil reserves are about 995 billion barrels.^[4] At present, the world consumes 24 billion barrels of oil every year, and the new oil exploration is getting less and less, only 5 billion barrels per year.^[4] Oil reserves outside the Middle East are declining and oil resources are limited. According to the estimates of the American Petroleum Industry Association, the amount of crude oil that has not yet been mined on the earth is less than two trillion barrels, and the time for human exploitation is no more than 95 years.^[6] Before the advent of 2050, the development of the world economy will increasingly rely on coal. Then between the year of 2250 and 2500, coal will be depleted and fossil fuel supplies will also be depleted.^[7]

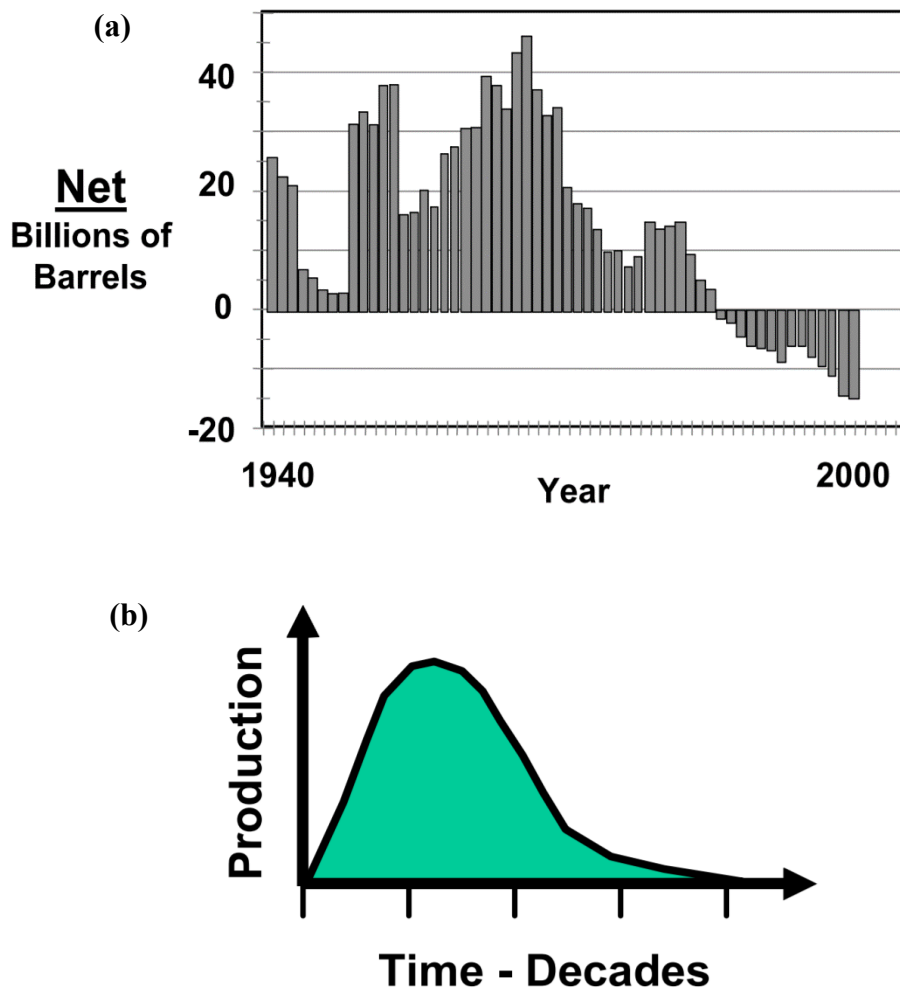


Figure 1. (a) The net billions of barrels of oil per year from 1940 to 2000, from the figure we conclude that the rate of world production of oil can not rival the rate of our consumption and (b) The tendency of oil production relate with time. ^[47]

In the face of global resources depletion, we must try to solve this situation. From decades, the clean and green energy resources came to our life. The definition of green energy should be: a clean, efficient, systematic application of energy technology systems. There are three implications: First, green energy is not a simple classification of energy, but refers to the technical system of energy use; second, green energy not only emphasizes cleanliness but also emphasizes economy; for the third green refers to certain emission standards. Green energy also includes renewable energy sources such

as hydropower, wind power, solar energy, bioenergy (biomass), and geothermal energy (including groundwater and water). There is no possibility of energy depletion in renewable energy sources. Therefore, the development and utilization of renewable energy sources are increasingly valued by many countries, especially in countries with energy shortages. Among those renewable energy, solar energy attracts scientist most attention because of its widespread, cleanness, enormous and versatility.

The sun can provide earth with tremendous energy. You may imagine, how much of energy exactly? Let`s put some statistics, in 1906, San Francisco had earthquake, with the magnitude 7.8, the earthquake released about 10^{17} joules of energy, that is the only 1 second of energy which sun delivered to earth; the petroleum on earth contain 1.7×10^{22} joules of energy, 3 trillion barrels of oil, which is only 36 hours of energy delivered from sun to earth; human being exhaust 4.6×10^{20} joules of energy per year, which is only 1 hour energy from sun to earth.^[2] As you see, the amount of energy provided by sun is impressive and if we develop proper technology, solar energy will no doubt replace the fossil. There are mainly three ways to utilize solar energy as shown in **Figure 2**: solar energy can convert to electricity at the presence of solar cell; it will generated fuels (hydrocarbon, hydrogen) through photosynthesis in green tissue of plant or photocatalysts synthesized by human being; sun light will produce heat for the future utilization. Despite huge amount and versatility of solar energy, we can only use little of them. The electricity from solar energy only accounts for 0.015% of the world`s electricity production; solar heat only accounts for 0.3% of heat production.^[8] The fuels or biomass generated from photosynthesis so far is the largest use in solar energy, human being usually burn the biomass to get energy, however the rate of replacing new

plants is far slower than we cut burn them. Not only this act will destroy environment but also generate air pollution.

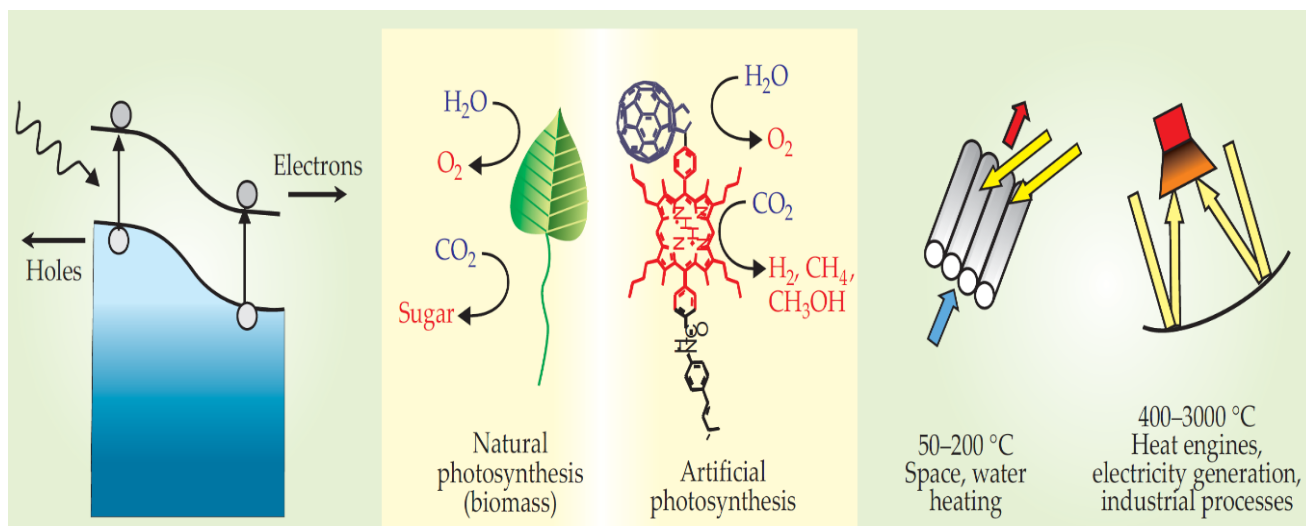


Figure 2. Three types of energy conversion from solar energy: electricity, fuel, heat.^[2]

Despite huge amount and versatility of solar energy, we can only use little of them. The electricity from solar energy only accounts for 0.015% of the world's electricity production, and solar heat only accounts for 0.3% of heat production.^[2] The fuels or biomass generated from photosynthesis so far is the largest use in solar energy, human being usually burn the biomass to get energy, however the rate of replacing new plants is far slower than we cut burn them. Not only this act will destroy environment but also generate air pollution. From decade, many scientists have tried to utilize more efficient solar energy. More efficient solar cell, which based on single-crystal silicon and whose efficiency can reach 18% or higher in solar energy conversion, had already been developed.^[2] In addition, artificial photosynthesis, which is inspired by plants or biomass, was widely investigated. Among all the investigation of solar energy conversion, the most promising is photochemistry. Solar fuels can be generated via artificial method, based on semiconductor photocatalyst. Its efficiency can be much

better than that of artificial photosynthesis, especially if the structure of semiconductor material with efficient solar energy conversion come true. In photoelectrochemical conversion, the photo-induced electron and holes pairs produced over the semiconductor materials can be used to split water into hydrogen or reduce carbon dioxide into hydrocarbon fuels at the surface of semiconductor photocatalyst with an electrolytic solution, rather than being sent through the external circuit.^[9]

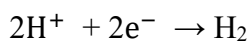
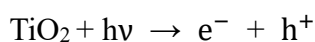
From discussion above, we can find semiconductor plays a significant role in the process of photochemistry. What is semiconductor, why this magic material can convert solar energy into biomass fuels? We will find the answer in the next chapter.

1.2 The semiconductor photocatalyst

When 1972 Fujishima and Honda published a paper about the Photolysis of water into hydrogen using TiO_2 as a photocatalyst, [10] which marked the beginning of the era of semiconductor photocatalyst. Since then, researchers in various fields began to investigate the process of photocatalyst. Over 40 years of development, photocatalysis under semiconductor has been Formed two main branches: environmental photocatalysis and solar energy conversion photocatalyst (mainly photocatalytic decomposition of water into hydrogen). Due to the worldwide problem of energy crisis and environmental pollution, this reaction has been receiving increased attention. Therefore, photocatalysis which utilize solar energy efficiently and transfer solar energy to other types of traditional energy (electricity, fossil energy) is the current hot spot of photocatalytic research. In addition since the reaction system of semiconductor photocatalytic oxidation can convert absorbed light energy into chemical energy under photocatalysis, many reactions which is previously difficult to achieve under normal condition can now be done under relatively mild conditions and proceeds smoothly in presence of photocatalysts. The use of sunlight and air can directly decompose many organic pollutants into small inorganic small molecules, carbon dioxide, and water. Such photocatalytic decomposition processes can mitigate pollution. Based on the prominent advantages of semiconductor multiphase photocatalytic oxidation in environmental protection, people have increasingly investigated it and its potential applications in depth.

The energy band structure of a semiconductor is usually made up of a low energy that is full of electrons valence band (VB) with an empty high energy conduction band (CB), the size of the distance between CB and VB is called the band gap. The photocatalytic properties of semiconductors are determined by their specific energy

band gap. When using the light energy ($E=h\nu$ where E is the energy of light, h is plank constant and ν is the frequency of specific kind of light) is equal to or greater than the semiconductor bandgap, the photocatalyst has begun. The electrons (e^-) in the valence band are excited to the conduction band and migrate to the surface of the particle under the action of an electric field, so that holes (h^+) are formed in the valence band, thereby generating a highly active electron/hole pair. The highly active photo-generated holes (h^+) has a strong oxidation ability and thus oxidize OH^- and H_2O which absorbed on the surface of photocatalyst into $\bullet OH$. The $\bullet OH$ radical have a strong oxidation ability which could react with much pollutant molecular. At the same time, the hole (h^+) itself can also seize the electrons in the organic substance adsorbed on the surface of the semiconductor, so that the substance that does not absorb light is directly oxidized and decomposed.^[11] These two types of oxidation may work independently or at the same time. There are different degrees of involvement of different oxidation methods for different substances. This is the example of photocatalytic degradation of pollutant. On the other side, the conduction band (CB) consist of highly active electron (e^-), which can serve as a reductive species. This is the basic mechanism of photocatalytic reduction ^[13] ^[14]. It applies to carbon dioxide reduction into hydrocarbon, which has a significant meaning in this world. Carbon dioxide is a greenhouse gas and full up in our atmosphere, if we use photocatalytic reduction to transfer CO_2 into energy – hydrocarbon, it will definitely mitigate our energy crisis. The following equations (equation set 1) and mechanism shows how semiconductor photocatalysts of TiO_2 can serve as redox reaction: ^[11]



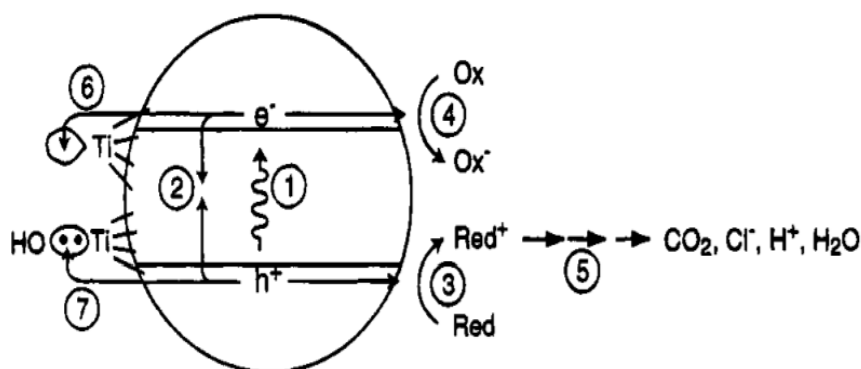
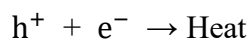
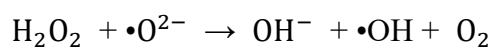
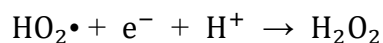
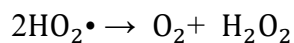
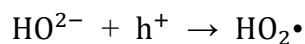
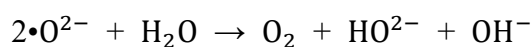
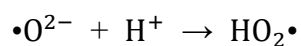
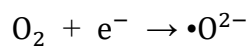


Figure 3. The steps in the photoelectrochemical mechanism: (1) formation of charge carriers by a photon; (2) charge carrier recombination to liberate heat; (3) initiation of an oxidative pathway by a valence-band hole; (4) initiation of a reductive pathway by a conduction-band electron; (5) further thermal (e.g., hydrolysis or reaction with active oxygen species) and photocatalytic reactions to yield mineralization products; (6) trapping of a conduction band electron in a dangling surficial bond to yield Ti(III) trapping of a valence-band hole at a surficial titanol group.^[11]

Common single compound photocatalysts are metal oxide or sulfide semiconductor materials (e.g. TiO_2 , ZnO , Fe_3O_4 , CdS , and ZnS). They have a large band gap and enable chemical reactions to be carried out over a wide range.^[15] The key factor

to photocatalytic degradation of organic matter is the reduction potential of $\text{H}_2\text{O}/\bullet\text{OH}$ ($\text{OH}^- = \bullet\text{OH} + \text{e}^-$, $E_g = -218 \text{ V}$) is smaller than band gap of desired photocatalyst and can stable for a long time.^{[11] [20]} In the aforementioned compound semiconductor material, polymorphs of metal sulfides and iron oxides are susceptible to photocathode corrosion affects its activity and lifetime and is therefore not the best photocatalytic material. The nature of the zinc oxide is not stable. The partially dissolved zinc hydroxide covers the surface of the zinc oxide particles and deactivates the catalyst. In contrast, TiO_2 is the most widely used photocatalytic material in the research due to its stable chemical properties, strong resistance to photo-corrosion, insolubility, non-toxicity, and low cost.^[17] It can make good use of ultraviolet rays below 390 nm in visible light without using short wavelength ultraviolet light emitted by expensive and harmful artificial light sources such as high-pressure mercury lamps. Hereby, TiO_2 has become the most promising green environmental protection catalyst. However, there are also imperfections. TiO_2 has a band gap of 3.2 eV, and its corresponding absorption wavelength is 387.5 nm. The light absorption is limited to the ultraviolet region.^[20] However, this part of the light does not reach the 5% of the surface solar spectrum, and the quantum efficiency of TiO_2 is not more than 28% at most.^[15] Therefore, the efficiency of solar energy is only about 1%, which greatly limits the use of solar energy. The goal of scientist is to promote the separation of photogenerated electrons/holes pairs and suppress their recombination, and thereby increase the quantum efficiency. At present, there are several kinds of commonly used semiconductor photocatalytic modification technology. It mainly includes transition metal ion doping ^[16], noble metal deposition, ^[16] doping of rare earth metal ions, compounding of semiconductor photocatalysts, ^{[18] [19]} and development of other novel photocatalysts.^[19] As a new type of water treatment technology, the semiconductor photocatalytic oxidation method has

made great achievements after several decades of development. However, it is still immature and there are still some problems. These are summed up as follows:

- (1) In the basic theoretical research, the current research on photocatalytic reaction mechanism still remains at the assumption and speculation stage. Therefore, the doping mechanism of semiconductors, the laws of movement and recombination of photoelectrons, and the relationship between the structure and reactivity of organic compounds are also not very clear, it needs to continue to focus on the discussion.
- (2) Although there are many kinds of photocatalysts that have been developed, most of the photon quantum efficiency is not high, the response range to light is narrow, and the catalytic ability in the visible light region is low and unstable. Therefore, the doping modification of the existing system is the development of new high-efficiency catalysts to achieve high photocatalytic performance in the visible light region and full use of solar energy sources will be an important direction for photocatalytic research.

As a photocatalyst for the treatment of organic contaminants and for organic and inorganic synthesis, semiconductors have received increasing attention and have developed rapidly. Although as an emerging technology, it is still immature, but the prospect is still broad. The essential problem of photocatalytic oxidation is still to seek an efficient photocatalytic reaction system, which requires the performance of the catalyst itself and the external conditions, especially the electron transfer system. The latter is often overlooked, and whether this photocatalytic reaction can sustained and rapid progress is particularly important. Because photocatalyst research involves many disciplines such as catalysis, materials, photochemistry, and the environment, it has considerable difficulties. Although there have been a lot of research work on

photocatalytic activity and stability at home and abroad. Great progress has been made, but there is still a certain distance from practical application. Therefore, photocatalysis And photocatalytic processes have to be applied in real life, and it is necessary to continue to carry out a large amount of research work in improving the activity and stability of the catalyst.

1.3 Introduction of graphitic carbon nitride

Until the 1980s, the formulation of the calculation formula for the solid elastic modulus of sphalerite started the research of C-N materials.^[21] In 1989, Cohen and Liu published an article based on the crystal structure calculation of β - Si_3N_4 in Science,^[22] predicting a carbon-nitrogen compound β - C_3N_4 with an elastic modulus comparable to that of diamond. They calculated that the elastic modulus of the compound is similar to that of natural diamond, and it is assumed that its hardness may be close to that of diamond. In 1996, Teter et al.^[24] recalculated C_3N_4 using the minimum energy pseudopotential method, and proposed five possible structures of C_3N_4 . They are α phase, β phase, cubic phase, quasi-cubic phase and graphite-like phase. At room temperature, the graphite-like C_3N_4 has the most stable structure. They calculated by theoretical calculation that except from g- C_3N_4 , the hardness of the other four C_3N_4 can be compared with diamond. The covalent interaction between carbon and nitrogen atoms in C_3N_4 is strong and relatively stable, and has a moderate energy bandgap of 2.7 eV. Therefore, after the carbon-nitrogen compound β - C_3N_4 covalent crystal was proposed, it attracted the attention a lot. g- C_3N_4 has a graphite-like layered structure in which C and N are both present in sp^2 hybridized form. N is interlaced and connected by δ bonds into a hexagonal structure. The interlayer is formed by a C_3N_4 ring or The C_3N_4 ring is composed of rings connected to each other by N atoms. g- C_3N_4 has two allotropes. One is formed by connecting triazines as structural units and the other is formed by connecting tri-s-triazines as structural units. Because of the different sizes of the nitrogen-containing pores in the structure, the two g- C_3N_4 allotropes lead to different electron environments for the nitrogen atoms, resulting in different stability of the two g- C_3N_4 species. Kroke et al.^[26] found that the tri-s-triazine-based g- C_3N_4 is more stable through density functional theory (DFT) calculations.

Therefore, in recent years, the tri-s-triazine structural unit $g\text{-C}_3\text{N}_4$ has been used for catalysis research.

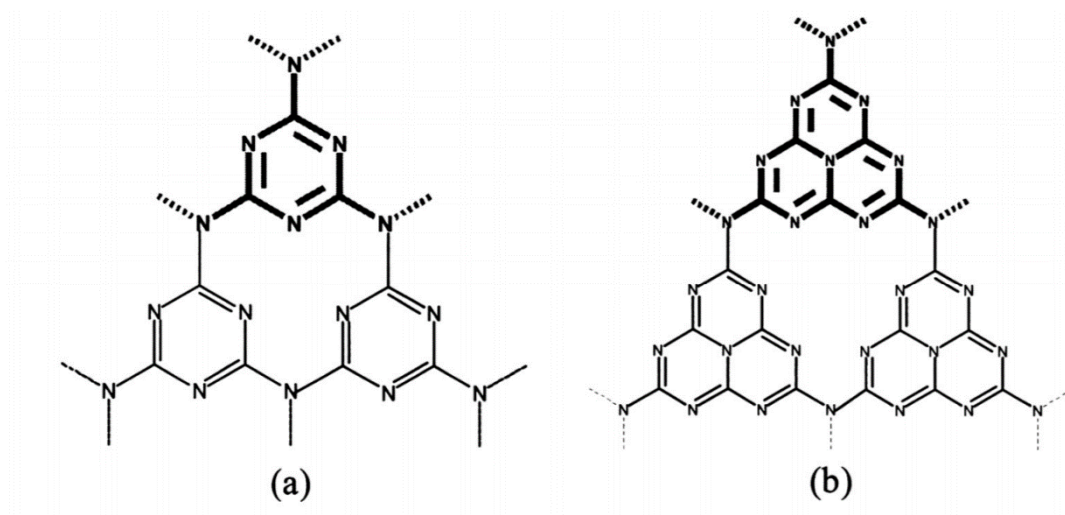


Figure 4. The chemical structure proposed for $g\text{-C}_3\text{N}_4$. (a) Triazine and (b) tri-s-triazine. ^[24]

In nature, natural carbon nitride crystals have not been discovered today, and experimentally prepared carbon nitride was also successfully prepared four years after the theoretical prediction. In 1993, Harvard University's laboratories used laser sputtering technology to artificially synthesize new materials that harder than diamonds. Analysis shows that the new material has $\beta\text{-C}_3\text{N}_4$ structure. Since then, scientists from all over the world have begun to study such low density and high hardness materials. The method of synthesize include thermal condensation, physical and chemical vapor deposition, electrochemical deposition, solvothermal synthesis, and pyrolysis of organics.

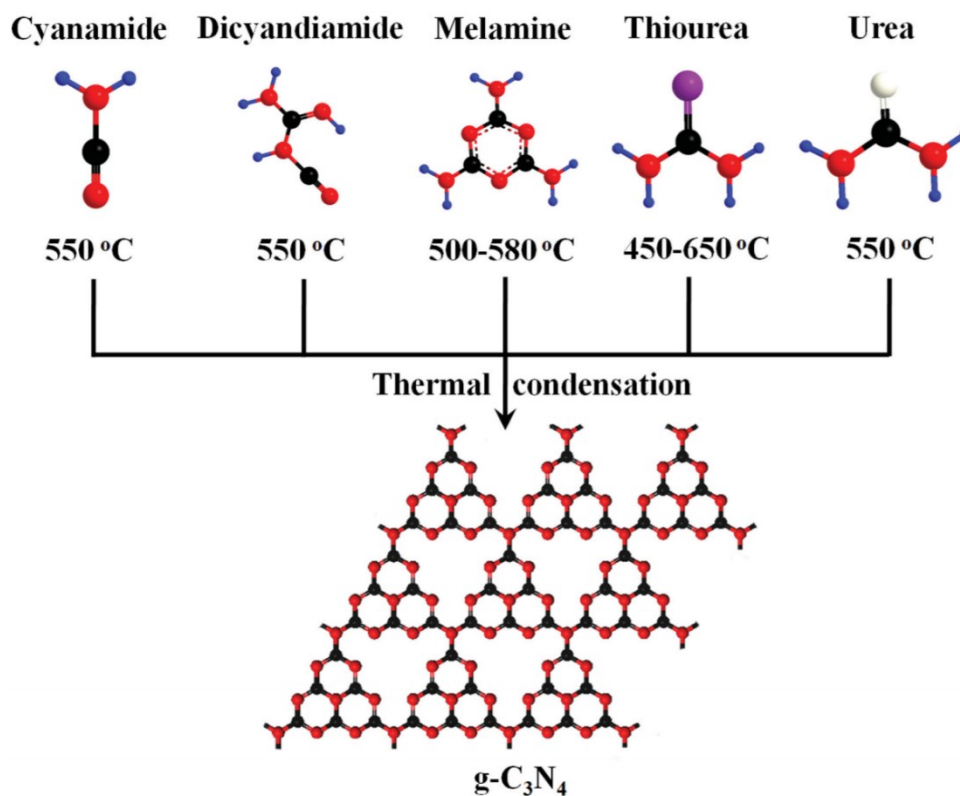


Figure 5. Schematic illustration of the main routes for the synthesis of g-C₃N₄ by condensation of cyanamide, dicyandiamide, melamine, thiourea and urea; the color code used in chemical structures: C, black; N, red; H, blue; S, purple; O, white.^[25]

As for application of g-C₃N₄, it is another type of semiconductor photocatalyst. However the most difference between g-C₃N₄ and TiO₂ is the small bandgap of g-C₃N₄, it is only 2.7 eV. With the CB and VB positions at -1.1 eV and +1.6 eV respectively vs normal hydrogen electrode (NHE).^[26] Unlike TiO₂, which is only photocatalytically active under the irradiation of ultraviolet, g-C₃N₄ is able to absorb visible light due to its small bandgap, which is a fantastic characteristic. With all the advantages as a photocatalyst mentioned above, g-C₃N₄ can be applied for photo-degradation of water into hydrogen,^[25] degradation of organic dyes,^[25] and organic catalytic reaction.^[25] Although g-C₃N₄ has the advantages described above, it still has some deficiencies. Because g-C₃N₄ itself has the characteristics of polymer materials, there is a small specific surface area as a photocatalyst; large bandgap; fast recombination of

electron/hole pairs and low efficiency of quantum utilization which greatly limits its application in the energy and environmental fields. So here are some ways to increase photocatalytic activity.

(1) Nano-modification of g-C₃N₄ materials: [27][28] [29] nano-modification of g-C₃N₄ can effectively overcome its small specific surface area, fast electron-hole recombination, and low quantum efficiency and other characteristics have received extensive attention. So far, the main methods for nanoc-modification include the template method or the non-template method. The template method includes a hard template method and a soft template method. Wang et al using SiO₂ nanoparticles as template, mesoporous g-C₃N₄ with different specific surface area and diameter was synthesized by adjusting the mass ratio of SiO₂ and cyanamide aqueous solution. The surface area and light absorption properties are improved to different extents, thereby increasing its photolysis hydrolytic hydrogen production activity. In addition, many different shapes of g-C₃N₄ have been synthesized by the hard template method, such as nanorods, hollow spheres and nanosheets.

(2) The doping of g-C₃N₄: [29] mainly include metal doping and non-metal doping. The non-metal doping mainly includes the doping of g-C₃N₄ by non-metals such as C, N, B, P, S, and F. Generally, it is believed that the C, N, and H elements in the tri-s-triazine structural unit are replaced by these non-metals. Substitution of elements, resulting in the formation of a lattice defect of g-C₃N₄, resulting in the efficient separation of photogenerated electrons and holes, leading to improved photocatalytic performance. Doping of metal elements mainly includes Fe, Ni, Cu, Zn, etc. It is generally considered that a small amount of metal ions are doped. In the g-C₃N₄ structural unit, it can serve as a electron sink for photoelectron and hole pairs, prolonging the recombination time of electrons and holes, thereby improving the photocatalytic performance of g-C₃N₄

(3) The combination of g-C₃N₄ and other material:^[30] photochemical and photophysical properties will change a lot after two or more semiconductor are combined.

In conclusion, Graphitic C₃N₄ as a photocatalyst have some unique character that other never have. Unlike TiO₂, which is only active in the UV region, g-C₃N₄ possesses a bandgap of 2.7 eV, this enable it to be a visible light-active photocatalyst. Since most of sun light reach to the ground is visible light. It is more valuable and worth to investigate. It is thermally stable even in air up to 550 °C, which can be attributed to its aromatic C–N heterocycles. Graphitic carbon nitride is chemically stable in most solvents such as water, DMF, THF, 0.1M NaOH. In addition due to the similar layered structure as in graphite, it has large surface area. It is obvious that large surface area will increase the efficiency of photocatalyst by scattering the light and provide more surface site for distributing reactant and product molecules.^[32] And g-C₃N₄ is only composed of two elements: carbon and nitrogen, suggest easy to prepare and its property can be tuned by simple strategy.

1.4. Introduction of tartrazine yellow

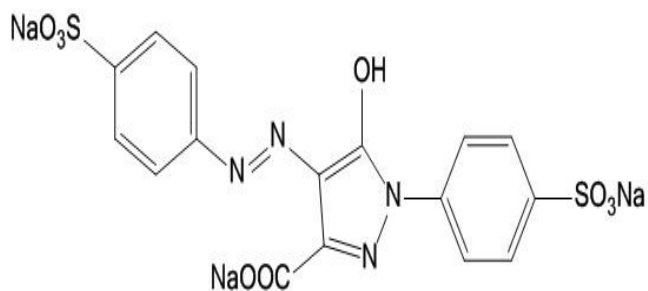


Figure 6. The molecular formula of tartrazine yellow and real object of tartrazine yellow. ^[39]

Food additives is important in our daily life. They allow us to enjoy a variety, delicious and safe food. It is hard to imagine the food without additives. Among them, pigment account for a large proportion of food additives. By the years of 1995, artificial or natural pigment was widely used in daily food, drugs or cosmetics. Natural pigment was usually derived from tissue of plants and flower but is not easy to extract. Artificial pigment was easy to get, which include Curcumin, Tartrazine, Sunset Yellow FCF, Carmines, Indigotine, Riboflavin. However, pigment only account for a small proportion in food, we should concern about it, because it may cause potential damage to our body. Among most pigments, due to the beautiful yellow color, simple synthesized, tartrazine is used extensively in product, which include: soft drinks, cotton candy, flavored chips, cereals, nachos, jam and jelly, some chew gum, even in shampoo, conditioner and soap. Drugs also include tartrazien. According to work of Walton et al.^[40], the ADI (Average Daily Input) is 7.5 mg/kg/day.

Tartrazine, also known as yellow 5, is a synthetic dye belonging to the group of azo dyes (N=N), it can be reduced into aromatic amine which is highly sensitive.^[41] The major metabolite is identified as sulfanilic acid.^{[40] [42]} This kind of artificial

pigment attribute to various of human diseases, including hepatocellular damage, ^[43] allergies, ^[44] headaches, ^[45] diarrhea and cancer in case of overdose.^[45] Thus, different and efficient ways of removing tartrazine and other pollutants from aqueous solutions, such as biological treatment, flocculation, precipitation, adsorption and photocatalytic processes are possible must be paid in attention.^[46]

In this thesis, in order to maximum the efficiency of photocatalytic activity, two simultaneous strategies were combined for modifying the $g\text{-C}_3\text{N}_4$, include developing a mesoporous structure, and deposition of Cu nanoparticles as a low-cost non-noble metal to decorate the surfaces of carbon nitride framework. We used melamine powder as a precursor which is inexpensive, easy to get and non-poisonous, SiO_2 gel as a hard template to create a mesoporous structure through a simple thermal condensation method. Two different value of copper nanoparticles were deposited on the surface of mesoporous carbon nitride (MCN) which are 5% and 10% through a simple precipitation-reduction method. To further investigate the photocatalytic activity, the sample of Cu-MCN were utilized in the photocatalytic degradation of tartrazine yellow as a hazardous dye in aqueous solution under UV-light irradiation. Also, it is the first time that tartrazine yellow is used for photocatalytic degradation by mesoporous carbon nitride, under UV light irradiation. We used several instrument to characterize the material, including X-ray diffraction (XRD), transmission electron microscope (TEM) and Thermogravimetric analyses (TGA). The results all shows good Phase structures, morphologies, and textural property. The result of photocatalytic degradation shows that Cu-MCN has good photocatalytic activity under UV light. Among six sample, 22 nm Cu(10)-MCN showed best photocatalytic activity, due to mesoporous structure and proper doping value. In addition, detailed mechanism was illustrate for explanation of photo-degradation of tartrazine yellow solution. Finally, the concluding remarks are

presented and some perspectives regarding the future development of g-C₃N₄ based photocatalysts are highlighted.

2. Experiment procedure

Materials before the experiment. All chemicals substance were purified in analytical grade and used without further purification. Distilled water was used for all solution. Melamine and ammonium hydrogen bifluoride (NH_4HF_2) was purchased from Alfa Aesar; copper(II) nitrate hemi (pentahydrate) $\text{Cu}(\text{NO}_3)_2 \cdot 2.5 \text{H}_2\text{O}$, sodium borohydride (NaBH_4) and tartrazine yellow was purchased from Sigma-Aldrich; 22 nm (40%), 47 nm (30%) LuDOX SM colloidal silica was also purchased from Sigma-Aldrich; 95% ethanol was purchased from Decon Laboratories, INC.

Preparation of mesoporous carbon nitride (m- C_3N_4). The m- C_3N_4 was synthesized by polymerization of mixing melamine molecules and different size SiO_2 under high temperature and in the presence of argon. In order to synthesis different pore size mesoporous carbon nitride, we used different particle size SiO_2 as a hard template, which are 22 nm (40%), and 47 nm (30%) respectively. In detail, 2 g melamine and 60 mL deionized water were added into 100 mL beaker and dispersed in ultrasonic bath for 20 min. Then the suspension was heated and stirred until melamine was all dissolved. 5 g 22 nm (40%) and 6.6 g 47 nm (30%) SiO_2 gel solution (make melamine and gel solution 1:1) was added into previous solution carefully through pipette. The mixture was heated at 80 °C and stirred in an open system for 3 h until water evaporate. Then the dried solid was ground into finite powder and calcined for 3 h in the presence of argon. The specific parameter of furnace is: ventilating the glass tube through argon for about 40 min in order to exhaust air, from room temperature to 550 °C, the heat up rate is 20 °C/min, heat the sample in the temperature of 550 °C for 3 h, then cooling the

furnace from 550 °C to room temperature. After calcining, the mixture solid is C_3N_4 and SiO_2 . Then, sample was ground into powder for future usage.



Figure 7. The mixture of C_3N_4 and SiO_2 .

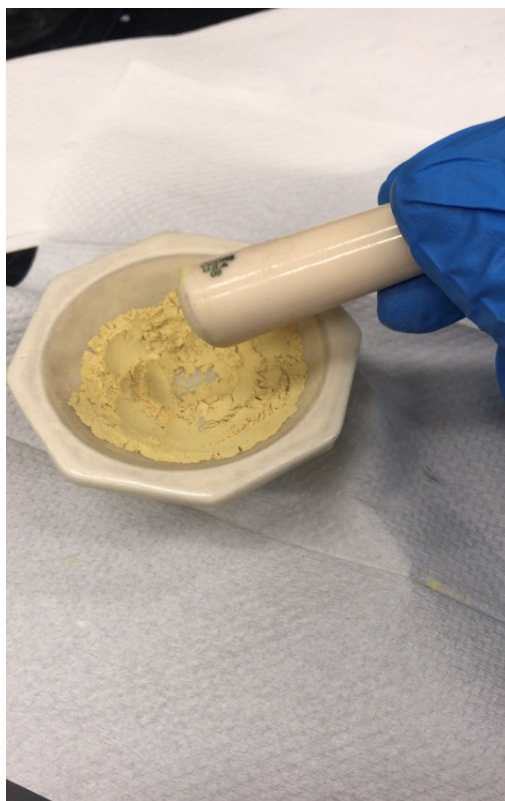


Figure 8. Ground the mixture into powder.

Removal of SiO_2 . Adding 13.5 g ammonium hydrogen bifluoride (NH_4HF_2) and 60 mL deionized water into a Teflon container, making the concentration into 4 mol/L. Adding the mixture of C_3N_4 and SiO_2 into container and stir for 48 h. After treatment the suspension was filtered and washed by deionized water 4 times, 95% ethanol for 2 times until pH of the liquid reached 7.0. Finally, collect filter cake and dried overnight in 70 °C. The result powder are 22 nm m- C_3N_4 and 47 nm m- C_3N_4 .



Figure 9. Removal of SiO_2 by NH_4HF_2 .



Figure 10. Filtering the suspension.



Figure 11. The sample of mesoporous carbon nitride.

Doping copper nanoparticle. The $\text{Cu}(x)\text{-m-C}_3\text{N}_4$ ($x\%$ denote the mass fraction of copper) was synthesized through precipitation-reduction method. 40 mL deionized

water added into 300 mg $m\text{-C}_3\text{N}_4$, the sample was in ultrasonic bath for 20 min making the suspension more uniform. Then adding a desired amount of Copper (II) nitrate trihydrate ($\text{Cu}(\text{NO}_3)_2 \cdot 2.5 \text{H}_2\text{O}$) into suspension. (In detail, %5 mass fraction-54.7 mg $\text{Cu}(\text{NO}_3)_2 \cdot 2.5 \text{H}_2\text{O}$; %10 mass fraction-108.75 mg $\text{Cu}(\text{NO}_3)_2 \cdot 2.5 \text{H}_2\text{O}$). Stirring the suspension until Copper (II) dissolve. A desired amount of sodium borohydride NaBH_4 solution dropwise add into the mixture (In detail, 10% mass fraction-100 mg NaBH_4 ; 5% mass fraction-50 mg NaBH_4 , NaBH_4 was dissolved in a tiny bottle). The reaction was under room temperature and stirred for 4 h. The obtained powder was filtered and washed by deionized water 4 times, by ethanol 2 times until pH reach 7.0. Finally the product was dried overnight under temperature of 70 °C. The sample denote as 22 nm $\text{Cu}(5)\text{-}m\text{-C}_3\text{N}_4$; 22 nm $\text{Cu}(10)\text{-}m\text{-C}_3\text{N}_4$; 47 nm $\text{Cu}(5)\text{-}m\text{-C}_3\text{N}_4$; 47 $\text{Cu}(10)\text{-}m\text{-C}_3\text{N}_4$. It is easy to distinguish $m\text{-C}_3\text{N}_4$ and $\text{Cu-}m\text{-C}_3\text{N}_4$, because the latter is darker.

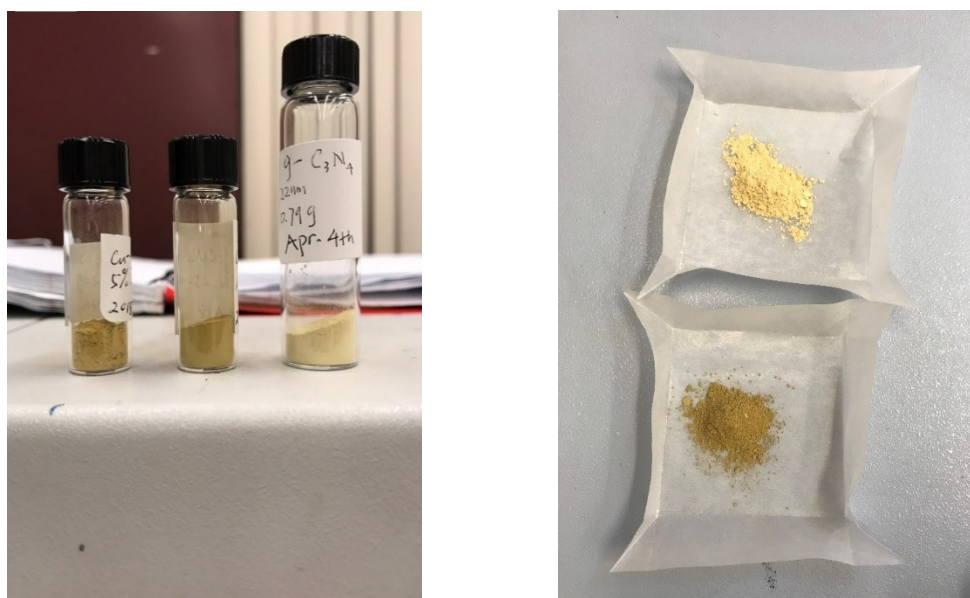


Figure 12. The sample of $\text{Cu-}m\text{-C}_3\text{N}_4$ and $m\text{-C}_3\text{N}_4$.

3. Characterization

The surface morphology including the pore distribution and the presence of copper nanoparticles was monitored through transmission electron microscope (TEM) (Topcon 002B TEM instrument). The operating voltage was 200 kV. The Micromeritics Tristar-3000 instrument (Micromeritics, made in USA) measure the pore properties and surface areas of the sample by N_2 porosimetry using liquid nitrogen (at $-196\text{ }^\circ\text{C}$). In detail, before each measurement, the sample was carried in a small glass tube and degas for 8 h under the presence of nitrogen, which will remove any possible impurities adsorbed on the samples' surfaces and fully dehydrate the sample. Based on the adsorption–desorption data, the pore size distribution and the surface areas of the samples were calculated using the Brunauer–Emmett–Teller (BET) method and the Barrett–Joyner–Halenda (BJH) method, respectively. The pore volumes of the sample were calculated in the base of how much amount of nitrogen (N_2) adsorbed at a relative pressure of 0.99. The measurement time takes about 12 h. X-ray diffraction (XRD) analysis of the sample were acquired through Philip XPert diffractometer (made in USA) operating with $\text{Cu K}\alpha$ radiation as the X-ray source. The X-ray diffraction (XRD) patterns were recorded using Philip X'Pert diffractometer operating with $\text{Cu K}\alpha$ radiation as the X-ray source in the 2θ of $5\text{--}80^\circ$. Thermogravimetric analyses (TGA) of the samples were measured using a PerkinElmer TGA7 instrument. The heating rate is $5\text{ }^\circ\text{C min}^{-1}$ and air flowing rate is 20 mL min^{-1} .

4. Photocatalytic activity procedure

The experiment of photocatalytic activity was carried as previous work.^[37] The prepared sample (Cu-m-C₃N₄) was carried on via monitoring the photocatalytic degradation of tartrazine yellow dye in an aqueous solution under UV light irradiation. The light source was provided by germicide lamp (Osram, German). The experiment of UV light photocatalytic activity was carried out by a 500 mL homemade Pyrex-glass reactor. Specifically, in order to keep the temperature of the reactor into room temperature, the body of the reactor was cooled by circulating water. The light source was positioned on top of the homemade reactor and the distance between the light source and the reactor was maintained at 10 cm. In the experiment, 100 mg photocatalyst was dispersed into 200 mL tartrazine yellow solution, in which the concentration of tartrazine yellow solution is 10 mg L⁻¹. Before the light irradiation, the suspensions were magnetically stirred in the dark box for about 60 min in order to obtain adsorption equilibrium before starting irradiation. The photocatalytic tartrazine yellow degradation was initiate with turning on the light source. At every interval of 30 min, 3 mL suspension was taken out from reactor and centrifuged for 10 min at 15000 rpm to fully remove the photocatalyst partical. Then the concentration of tartrazine yellow was measured by UV-vis spectrophotometer (Agilent, Cary 50). In order to test the photo-degradation efficiency, two equation can be used:

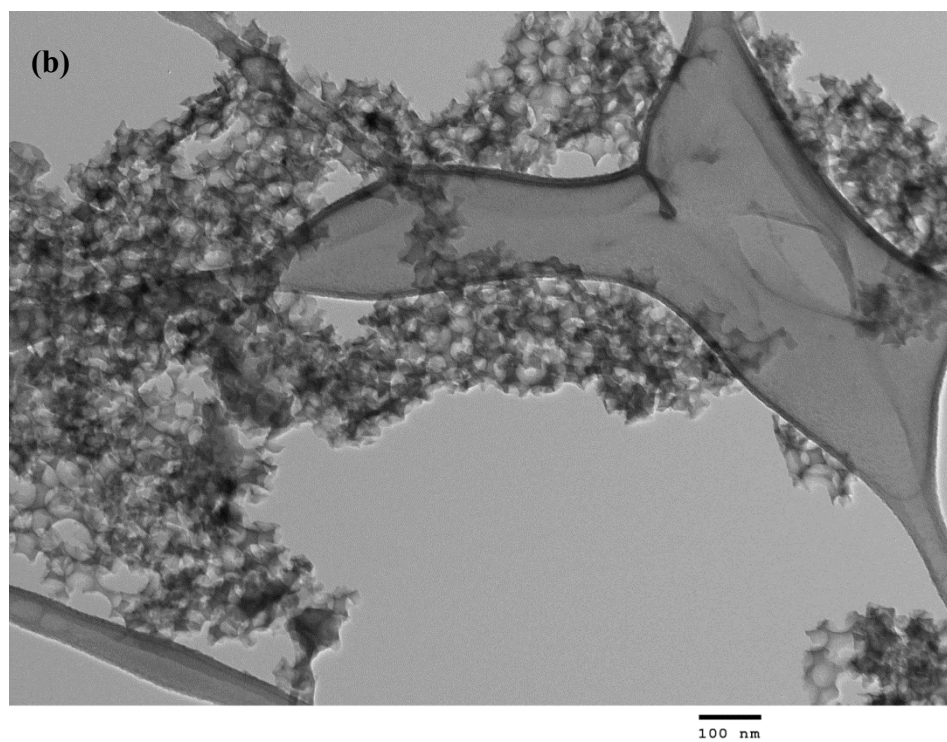
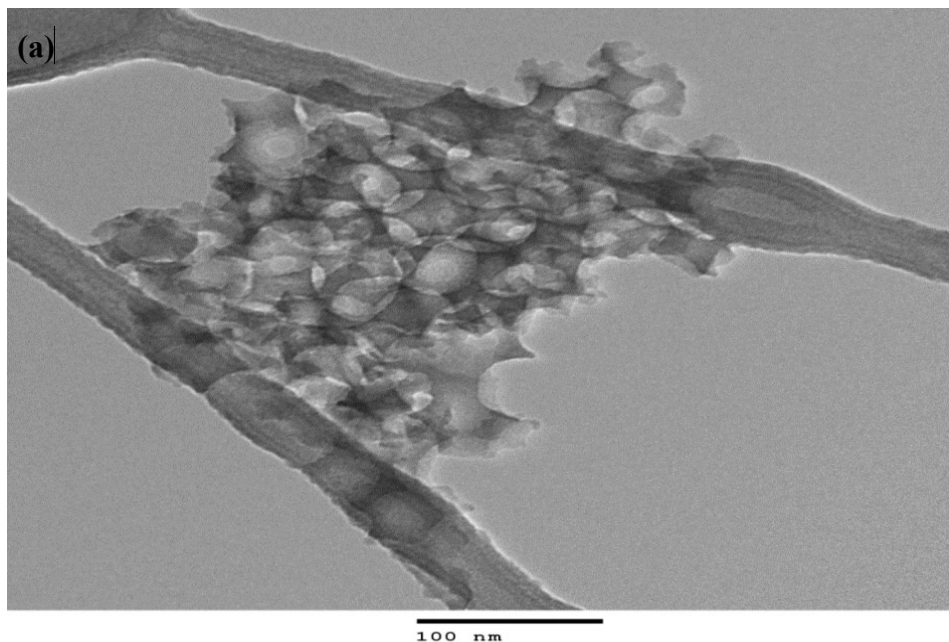
$$\eta = \frac{c_0 - c_t}{c_0} \times 100\% \quad \text{equation 2.}$$

$$\ln \frac{c_0}{c_t} = k_{app} t \quad \text{equation 3.}$$

Where c_0 and c_t are the initial and time dependent concentration of tartrazine yellow over photo-degradation, respectively. k_{app} is the pseudo first order reaction rate constant (min^{-1}), and t is the photo-degradation time (min).

5. Result and discussion

5.1 Transmission electron microscopy (TEM) analysis



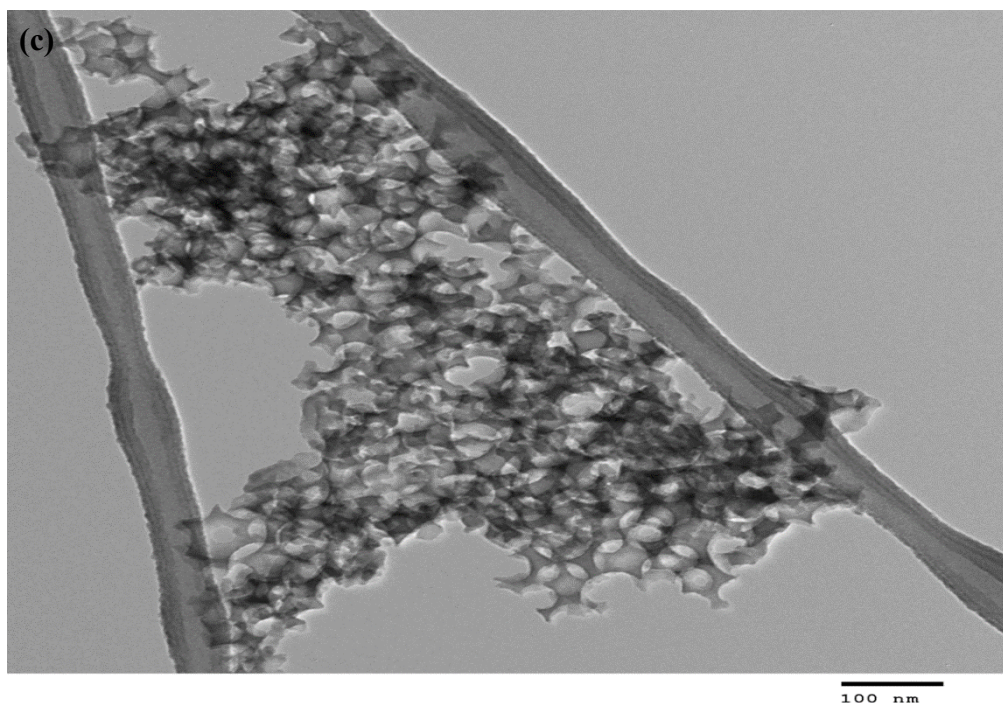


Figure 13. (a) Transmission electron microscopy (TEM) image of 47 nm m-C₃N₄ and (b) (c) transmission electron microscopy (TEM) image of 47 nm Cu(10)-m-C₃N₄.

Transmission electron microscopy (TEM) was used to investigate the structure and morphology of prepared material. In **Figure 13**, the TEM image imply that the m-C₃N₄ and Cu-m-C₃N₄ sample which derived from treatment with the colloidal silica have the presence of a well-developed mesoporous system with a uniform pore size. In **Figure 13 (a)**, the m-C₃N₄ shows clear a multi-pores system, the pore size and distribution is the reverse replica of silica template. Because the sample suspension is magnetically stirred, the pores distribution is uniform, and the diameter of the pores is consistent with size of silica gel, the BET test will confirm this viewpoint. We should notice that the size of silica gel should be appropriate for synthesis of m-C₃N₄. If the diameter of SiO₂ too small, thus the pore size will be small too, and the surface area will not increase; if diameter too big, the pore will be deform and collapse and have no improve for photocatalyst. **Figure 13 (b) and (c)** is TEM pattern of copper doping m-C₃N₄. It is

obvious that there were some black spot on the surface of mesoporous material. However we can not find a uniform distribution of copper particles doping on the m-C₃N₄, for some part of material, we can not find copper particles.

5.2 X-Ray diffraction (XRD) pattern

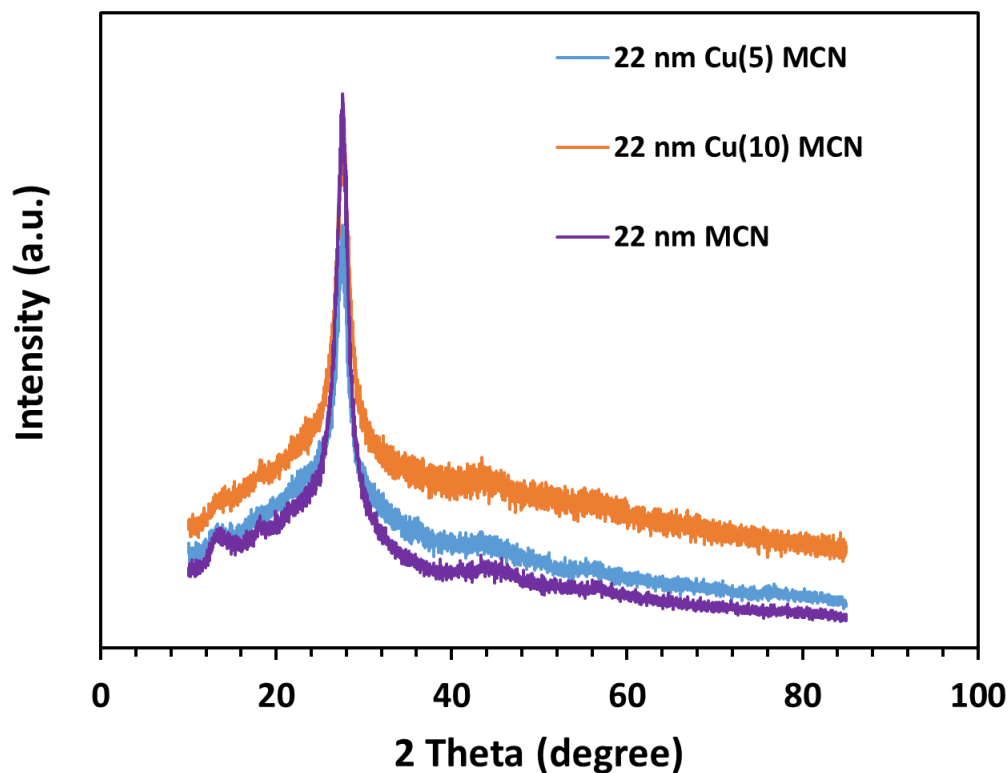


Figure 14. XRD pattern of synthesized sample.

The X-ray diffraction (XRD) patterns were used to test the chemical structures of the synthesized material. **Figure 14** shows the XRD patterns of 22 nm MCN, Cu(5)-MCN and Cu(10)MCN particles. In this figure, we will discover there are two major characteristic peaks, which is an intense peak, the other is a minor peak. The strongest XRD peak at 27.4° is a characteristic peak which suggest the interlayer stacking of aromatic systems, with the corresponding d-spacing of 0.326 nm.^[32] The minor peak around 13.1° which indicate an in-plane structural packing system which corresponding to a distance of $d = 0.687$ nm.^[32] However, the d-spacing is smaller than the size of tris-s-triazine molecule. It is probably because a portion of structure in MCN framework is deformed because of N–N repulsion.^[33] From **Figure 14**, we can also find, the

characteristic peak around 13.1° is decreased when we increase the doping copper value from 5% to 10%. In the sample of Cu(10) MCN, we can barely find the minor peak, while the peak in sample pure MCN is easy to find. This is because the copper nanoparticle will anchor on the outer and inner surface of the mesoporous structure thus the in-plane structure will be disrupted. In addition, there are no notable characteristic peaks corresponding to copper metal in this XRD pattern. The reason for it can be explain small value of doping copper particle.

5.3 Thermogravimetric analyses (TGA) of the materials

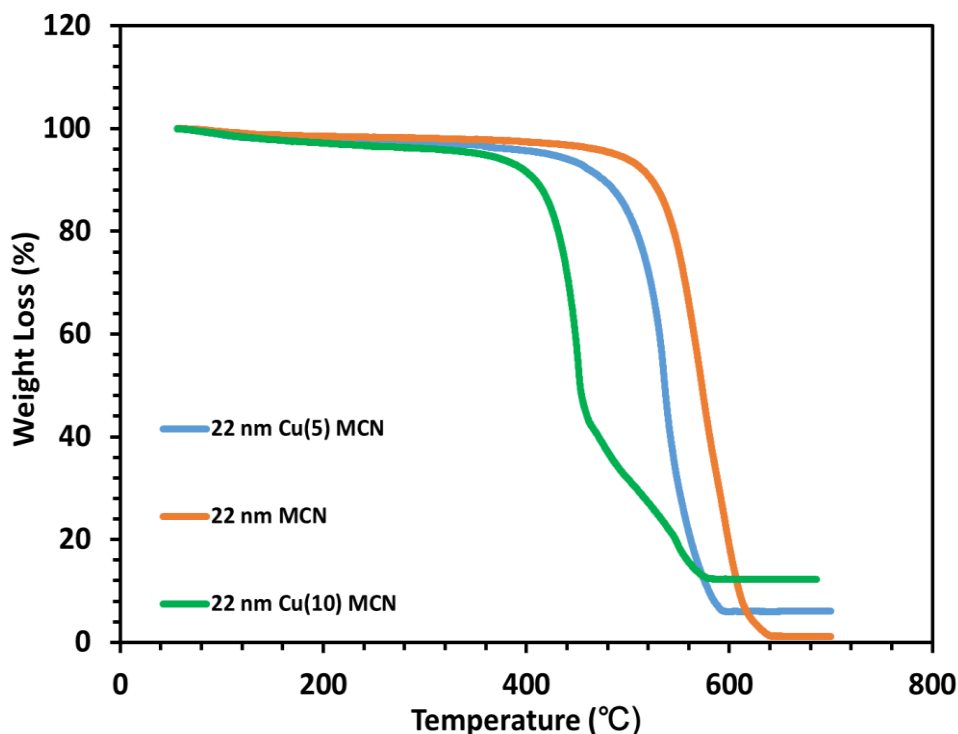


Figure 15. TGA plot of 22 nm Cu(5)-MCN Cu(10)-MCN and 22 nm pure MCN.

With Thermogravimetric analysis (TGA) of the sample (22 nm Cu(5)-MCN Cu(10)-MCN and 22nm pure MCN), we notice that with the sample will decomposed entirely when the temperature over 500 °C, which consistent with reference. We should take a notice of 22 nm Cu(5)-MCN, because 5% amount of copper particle doping on the surface of pure MCN, there is a little amount of residue according to the curve. According to the original data, 6.936 mg sample put in the, after heating for 129 min, there were only 0.420 mg residue. Since the sample was heated in the air, which exist oxygen, we speculate that the residue was CuO. Now we calculate the percentage of copper value. The molecular mass of Cu and CuO is 64 and 80 respectively.

$$0.420/6.936=0.060=6.06\%$$

$$6.06\% \times \frac{64}{80} = 4.85\%$$

Thus the actual value of doping Cu is wt. % 4.85, which is close to the theoretical value.

For Cu(10)-MCN the residue of sample was 0.933815 mg, we can calculate that :

$$0.933 / 7.626 = 12.24\%$$

$$12.24 \times \frac{64}{80} = 9.80$$

Thus the actual value of doping Cu is wt. % 9.80, which is consistent with theoretical value. With burning the sample of pure MCN for 129 min, according to the curve, we find almost no residue left. This suggests our synthesized 22 nm MCN is pure and decomposed in high temperature.

5.4 The specific surface area and pore size distribution

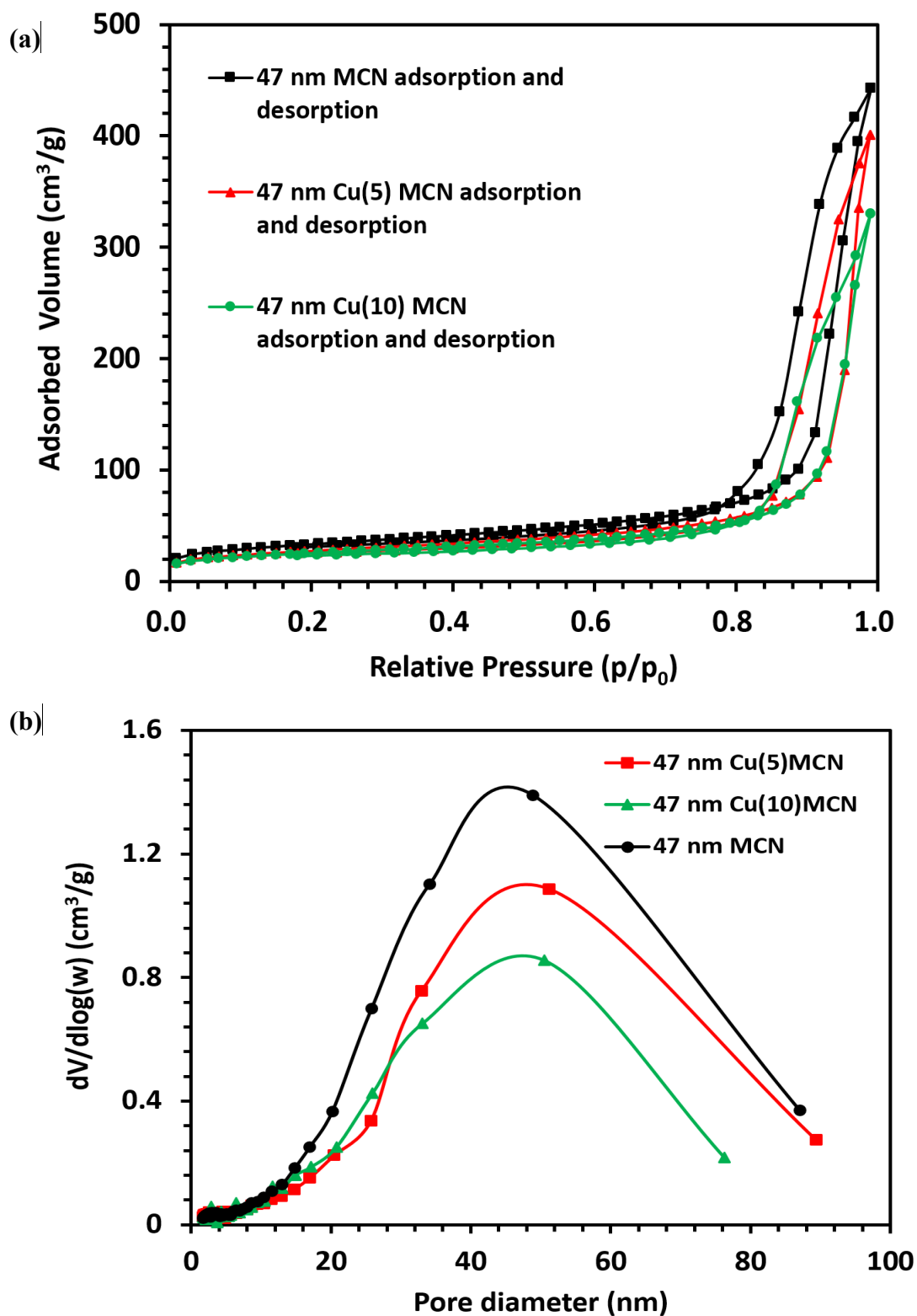


Figure 16. (a) N_2 adsorption-desorption isotherms of 47 nm Cu-MCN, 47 nm Cu(5) MCN and 47 nm Cu(10)-MCN and (b) pore size distributions of 47 nm MCN, 47 nm Cu(5)/MCN and 47 nm Cu(10) MCN.

Table 1. The surface area of synthesized sample.

Sample	BET surface area (m ³ /g)
22 nm C ₃ N ₄	128
22 nm Cu(5)-C ₃ N ₄	102
22 nm Cu(10)-C ₃ N ₄	93
47 nm C ₃ N ₄	116
47 nm Cu(5)-C ₃ N ₄	95
47 nm Cu(10)-C ₃ N ₄	87

Generally speaking, the mesoporous system and high surface area in a photocatalyst will definitely enhance the efficiency of the photocatalytic activity. Because it will increase light harvesting ability through scattering the light in their mesoporous system and larger surface area will provide more surface sites for distributing reactant molecules and product through porous networks and thus increase the photocatalytic activity.^[34]

Figure 16 (a), (b) shows the nitrogen adsorption/desorption isotherms and the corresponding curves of pore size distribution. The nitrogen adsorption/desorption isotherms is used to test the specific surface area of each sample and we test all 6 sample and table 1 recorded all specific surface area of six samples. We only put three sample on the figure because if put too many samples on figure, it will look in a mess. **Figure 16** (a) is three typical nitrogen adsorption-desorption isotherm, we can noticed that that these three samples curve have isotherms of type IV^[31] with hysteresis loops of type H3^[31] according to the IUPAC classification, which indicate there is a mesoporous sytucture in our sample.^[31] In detail, the hysteresis loop in the sample of MCN and Cu(5)MCN is due to the capillary condensation happened in mesoporous system, and

restrict nitrogen adsorption at high p/p_0 , which means these three samples have a more narrow pore size distribution and uniform pore distribution. **Table 1** records the surface areas of 6 samples. Two points should be noticed: the first is the surface area will be decreased, after doping copper particles. This is because the copper particles will anchor on the surface of pure MCN and some portion of Cu nanoparticles will block the pores, thus decrease the specific surface area. The second is the specific surface area of three 22 nm is larger than that of three 47 nm samples, that is because a portion of pores are collapsed or deformed when the pore size is too large. **Figure 16 (b)** indicates the pore diameter of three samples. The pore size was achieved by BJH method and with a peak about 50 nm, which is a reverse replica of 47 nm silica gel when we did the experiment. Therefore with the figure of pore size distribution, we can confirm that, we successfully develop the desired pore size as we expected.

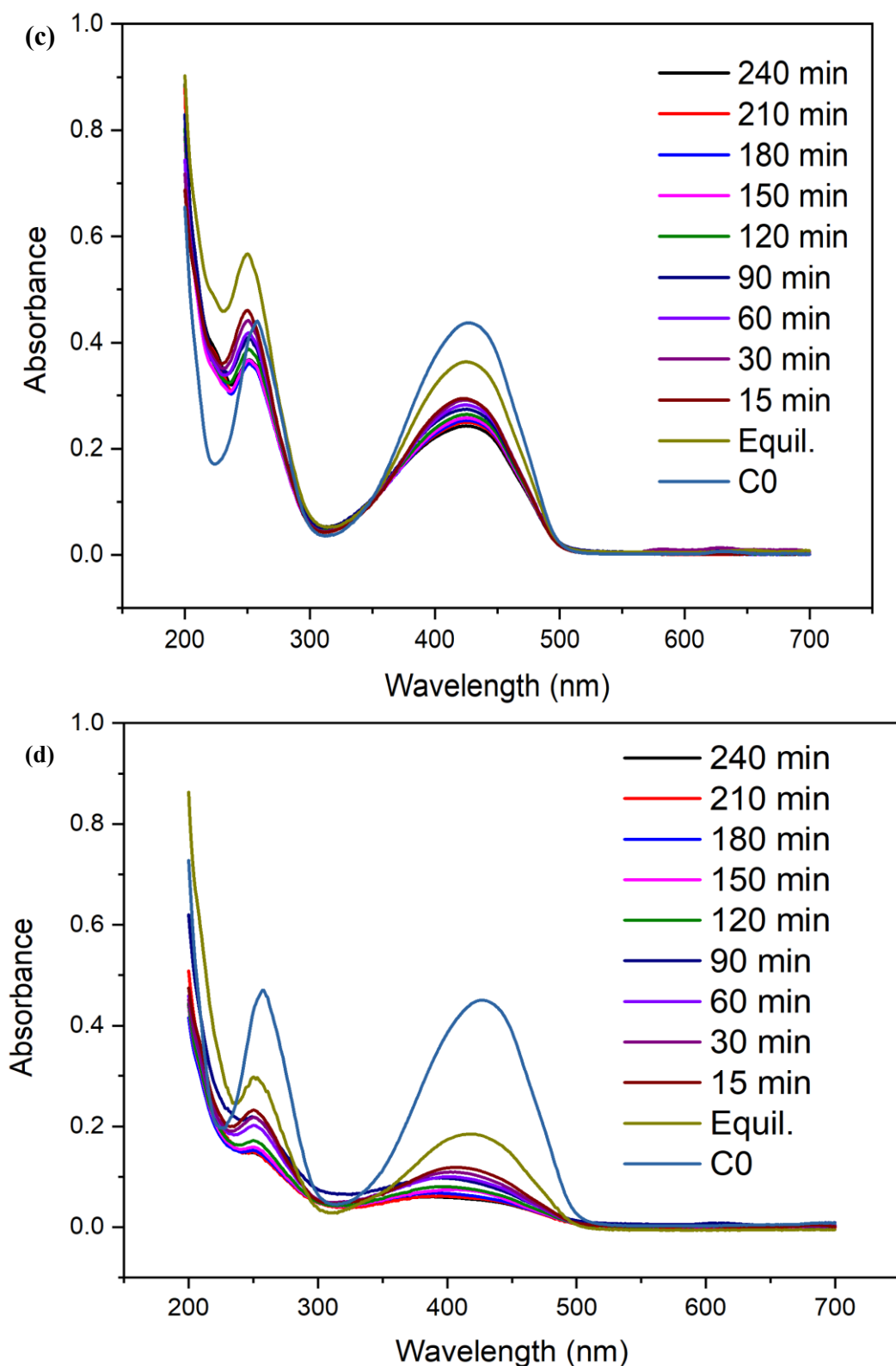


Figure 17. (a) The photocatalytic degradation of tartrazine yellow over bulk CN, 22 nm MCN, 47 nm MCN, 22 nm Cu(5) MCN, 22 nm Cu(10) MCN, 47 nm Cu(5) MCN and 47 nm Cu(10) MCN photocatalysts. (b) (c) (d) Time-dependent UV-vis absorption spectra for the catalytic degradation of tartrazine yellow over the 22 nm MCN, 22 nm Cu(5) MCN, 22 nm Cu(10) MCN photocatalyst.

Table 2. The mass of each sample.

Sample	Mass (g)
22 – C ₃ N ₄	0.1007
22 – 5% C ₃ N ₄	0.1007
22 – 10% C ₃ N ₄	0.1005
47 – C ₃ N ₄	0.1006
47 – 5% C ₃ N ₄	0.1004
47 – 10% C ₃ N ₄	0.1008

Table 3. The photodegradation extent for 240 min over 6 sample under the irradiation of UV light (sample 1 to sample 6 denote as 22 nm MCN, 22 nm Cu(5) MCN, 22 nm Cu(10) MCN, 47 nm MCN , 47 nm Cu(5) MCN and 47 Cu(10) MCN).

Time (min)	degradation rate of sample 1	degradation rate of sample 2	degradation rate of sample 3	degradation rate of sample 4	degradation rate of sample 5	degradation rate of sample 6
0	0	0	0	0	0	0
15	2.69	20.717	45.448	2.891	15.131	19.52
30	6.33	21.397	52.564	2.448	18.019	22.605
60	10.645	24.061	58.397	8.205	20.77	31.699
90	13.693	26.458	61.794	10.14	21.596	29.491
120	15.545	29.329	70.128	12.331	25.126	33.675
150	17.608	31.223	71.795	14.289	31.729	34.875
180	20.047	32.554	78.205	14.919	31.976	35.427
210	21.665	32.619	81.192	16.807	32.087	36.766
240	23.118	33.732	83.859	18.718	33.729	43.482

In the experiment, 0.2 g tartrazine yellow powder was dissolved in 200 mL water to solution 10 mg L^{-1} , added 0.100 g of catalyst to the tartrazine yellow solution, the mass of each sample is given in the **Table 2**. Before irradiation, the solutions were kept under magnetic stirring for 60 min in the dark to establish the adsorption equilibrium. During the irradiation, aliquots of 3.0 mL were sampled every 30 min and measurements were carried out by a UV-vis spectrophotometer.

Figure 17 and Table 1 are the results of photocatalytic activity which represent by photo-degradation of tartrazine yellow. **Figure 17** (b) (c) (d) is time-dependent UV-vis absorption spectra for the catalytic degradation of tartrazine yellow over the 22 nm MCNS, 22 nm Cu(5) MCN, 22 nm Cu(10) MCN photocatalyst. The x axis denote the wavelength of light and y axis denote absorbance, the bigger the concentration of tartrazine yellow, the higher absorbance. Different colors represent different time under photocatalyst. From **Figure 17** (b), after 240 min of irradiation the absorbance is still pronounce which means the concentration of tartrazine yellow is still pretty high, we can calculate the actual concentration of tartrazine yellow each time through calibrate curve. From **Figure 17** (c), after 240 min of irradiation, there is an obvious decline on absorbance, which we will know some of tartrazine was decomposed. As for **Figure 17** (d), after 240 min of irradiation, the absorbance reached near zero, which indicate most of the tartrazine was decomposed. Therefore, we will conclude that with increasing the loading of Cu particles from 0 to 10 wt. %, the photocatalytic activity increase gradually. When the loading value reached 10, the efficiency of photo-degradation reached highest.

Table 3 recorded all the data we needed. Two facts can be concluded. The first is no matter which pore size distribution, as long as increasing the doping copper value, the efficiency of photocatalyst will increase. This is because the copper nanoparticle

will serve as an electron sink, which will inhibit the recombination of electron and hole pairs. The second is the photocatalytic efficiency of three sample of 22 nm pore size is higher than those of 47 nm. That is because 22nm have bigger specific surface area. Which will increase the light harvesting ability as well as provide more surface site for distributing the reactant molecule into its porous network.^[31]

Figure 17 (a) will more clearly show the relationship between the efficiency of photocatalytic and each sample. The X axis represent irradiation time. Y axis is the ration of time-dependent concentration of tartrazine yellow and the original concentration. We also add a curve of bulk C₃N₄, which is a comparison. The bulk carbon nitride without any modification showed low photocatalytic degradation of tartrazine because of its small specific surface area and fast recombination of electron and hole pairs. From **Table 3** and this **Figure 16** (a), there is no doubt that develop a mesoporous structure and loading copper particle will increase the efficiency of photo-degradation for tartrazine yellow.

5.6 Possible photocatalytic mechanism

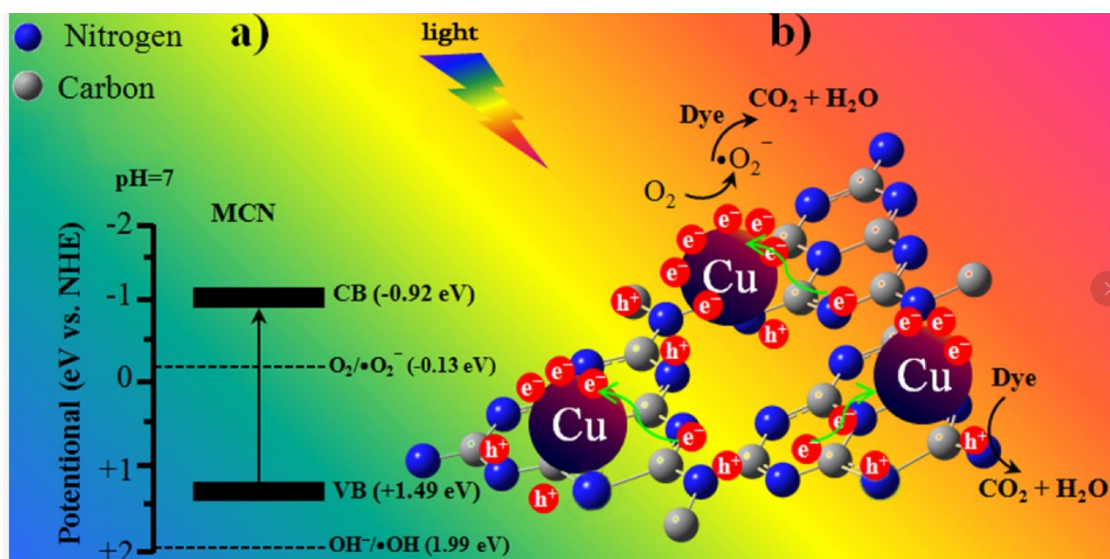


Figure 18. Mechanism of photocatalytic degradation of dye solution over the Cu/MCN photocatalyst. ^[31]

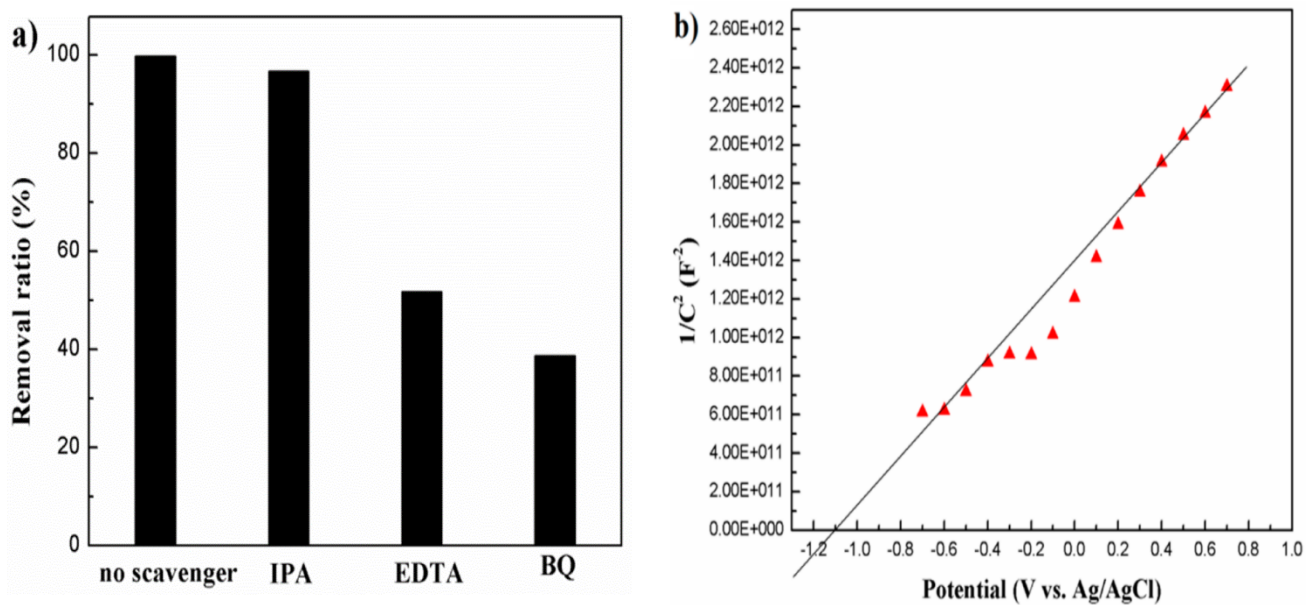
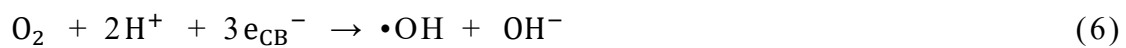


Figure 19. (a) Trapping experiment and (b) the Mott-Schottky plot for the MCN sample. ^[31]

In order to better explain the mechanism of photo-degradation of tartrazine yellow. Herein, I will use the work of Jourshabani M. et al.^[31] During the process of photo-degradation, Oxygen in the atmosphere will combine with electrons to create super oxide radical; and photo-generated holes will capture electrons from hydroxyl iron to produce hydroxyl radicals (Equation 4–6). These species play a significant roles during the process of photodegradation. The active species originated from the photocatalytic system include photogenerated holes (h^+), superoxide radicals ($\bullet O_2^-$), and hydroxyl radicals ($\bullet OH$).^[31] Also from the work of Jourshabani M. et al. we will further illustrate the mechanism of photocatalytic degradation over Cu/MCN photocatalyst. Trapping experiment ^[31] was utilized here. The active species involves photogenerated holes (h^+), superoxide radicals ($\bullet O_2^-$), and hydroxyl radicals ($\bullet OH$) can be traced by isopropanol (IPA), benzoquinone (BQ), and ethylenediaminetetraacetic (EDTA) as the $\bullet OH$, $\bullet O_2^-$ and h^+ scavengers, respectively. As can be seen in **Figure 19. (a)**, after adding IPA, the efficiency of photo-degradation of dye solution was unchanged, which means $\bullet OH$ radicals are unimportant or we can say never exist in the degradation of tartrazine yellow by Cu/MCN. However, after adding the BQ and the EDTA in the solution, the photo-degradation efficiency of dye solution is significantly declined, which indicate the photo-generated h^+ and $\bullet O_2^-$ are the major active species. Based on the above results from the tracing experiments, the h^+ and $\bullet O_2^-$ radicals as the major oxidate species during the process of photocatalytic degradation over Cu/MCN catalyst under the light irradiation, while the role of photogenerated $\bullet OH$ is not important.

So let's have a look why hydroxyl is unimportant or never exist in the photocatalyst of C_3N_4 . **According to Figure 18**, the CB and VB of MCN is -1.1 and $+1.31$ eV respectively. And the bandgap of it is 2.41 eV. The reason why hydroxyl

radicals have a very little role in the photodegradation efficiency of the Cu/MCN is probably that the standard redox potential of $\bullet\text{OH}/\text{OH}^-$ is +1.99 which is higher than the valence band VB potential energy of the MCN. Therefore, the photogenerated h^+ cannot oxidize OH^- to produce $\bullet\text{OH}$ radicals. On the other hand, the standard redox potential of O_2 and $\bullet\text{O}_2^-$ pair is -0.13, which is lower than MCN CB potential, as a result, the photo-generated electrons will reduce the oxygen to produce super oxide radicals. That is why the active species in our reaction is only photo-generated holes and super oxide radical.



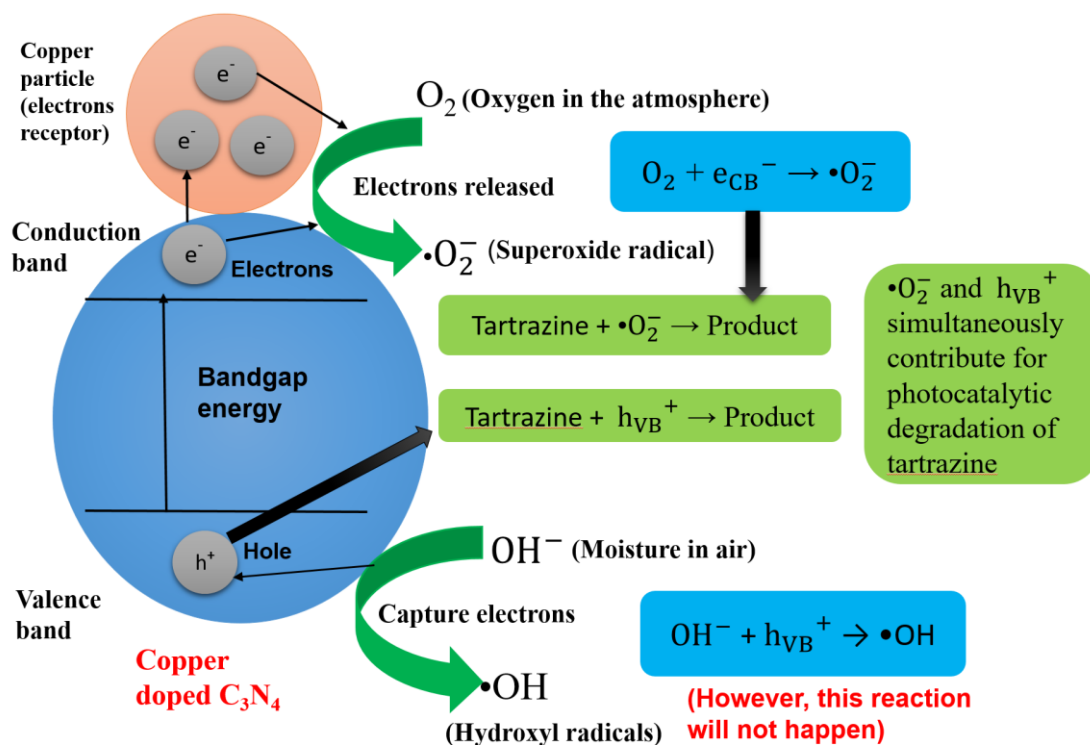


Figure 20. Detailed possible mechanism of photo-degradation of tartrazine yellow by Cu/MCN

So let's summarize the facts about photo-degradation of tartrazine yellow over Cu-MCN. As shown in **Figure 20**, after absorbing enough light energy, electrons will be excited from valence band to conduction band and leave the holes in valence band which contain positive charge. At this time some reaction will take place on the surface of Cu-MCN. Traditionally, like some semiconductor photocatalysts, in the surface near valence band, each h^+ captures one electron of hydroxyl ion and produces hydroxyl radicals, however this reaction will not happen here, because the standard redox potential of hydroxyl iron and hydroxyl radical is too large, and h^+ are not able to oxidize hydroxyl iron into hydroxyl radicals. On the other side, the oxygen in the atmosphere will combine with electrons and form superoxide radicals. So in the presence of Cu-MCN, the photo-generated holes and superoxide radicals will together serve as active species and oxidize tartrazine yellow molecule into final product.

6. Conclusions

In summary, this thesis mainly focused on the synthesis of graphitic carbon nitride material through two separate process which include developing a mesoporous structure, and loading desired amount of Cu nanoparticles as an inexpensive, easy-get non-noble metal on the surface of carbon nitride. During the process of synthesizing mesoporous carbon nitride, we used melamine as a precursor which is inexpensive and non-poisonous and silica gel as a hard template by calcine the mixture for 4 hours. Then, two desired amount of copper nanoparticles were decorated on the surface of MCN. We used a simple precipitation reduction method to achieve it. We also used several method to characterize our sample, including transmission electron microscope (TEM), X-ray diffraction (XRD), the pore size distribution and the surface areas of the samples using the Brunauer–Emmett–Teller (BET) method and the Barrett–Joyner–Halenda (BJH) method and Thermogravimetric analyses (TGA). The photocatalytic activities were investigated by the photo-degradation for tartrazine yellow under the presence of Cu-MCN. According to the time dependent UV–vis spectrophotometer, with increasing the loading of Cu particles from 0 to 10 wt. %, the photocatalytic activity increase gradually. When the loading value reached 10, the efficiency of photo-degradation reached highest. Increasing the specific surface area will also increase the efficiency of photo-degradation. The highest degradation extent of tartrazine yellow was over 80% after 240 min of irradiation. The bulk graphitic carbon nitride showed low photocatalytic activity, due to its small specific surface area and fast recombination of electron and hole pairs. The photocatalytic mechanism was also discussed in detail, it explain the major active species in this reaction and illustrate why copper nanoparticle can inhibit the recombination. As a result, It is obvious, develop a mesoporous structure

and decorate copper nanoparticles will enhance the efficiency of photocatalytic activity. In addition, carbon nitride serve as a semi-conductor which bandgap is small have a broad application, the photo induced electron-hole pairs can be served as active species in redox reaction, for instance the reduction of carbon dioxide into hydrocarbon. In the future, the carbon nitride will have a brighter tomorrow, researchers will find a more efficient way to harness this economical-friendly material.

There is also some defect in my thesis. The light source in the experiment is ultra-violet, not visible light. It was a pity, because not many semiconductor photocatalyst is visible light active. In my lab there isn't any visible light bulb as light source which I have to ultra-violet source. If I can achieve photo-degradation under visible light, this thesis will definitely attract much more attention. But no problem, someone else will make my dream come true someday.

7. References

- [1] Weisz, P. B. Basic choices and constraints on long-term energy supplies. *Phys. Today* **2004**, 28-35.
- [2] Carbtree, G. W.; Lewis, N. S. Solar energy conversion. *Phys. Today* **2007** 37-42.
- [3] Kamat, P. V. Meeting the clean energy demand: nanostructure architecture for solar energy conversion *J. Phys. Chem. C* **2007**, 111, 2834-2860.
- [4] Bartlett, A. A. Sustained availability: A management program for nonrenewable resources. *Am. J. Phys.* **1986**, 54, 398-402.
- [5] Myers, N.; Kent, J. New consumers: The influence of affluence on the environment. *Proc. Natl. Acad. Sci. U.S.A.* **2003**, 100, 4963-4968.
- [6] Campbell, C. J. Industry urged to watch for regular oil production peaks, depletion signals. *Oil Gas J. Tulsa* **2003**, 101, 38-44.
- [7] Campbell, C. J.; Laherrere, J. H. The end of cheap oil. *Sci. Am.* **1998**, 278, 60-65.
- [8] Dresselhaus, M. S.; Thomas, I. L. Alternative energy technologies. *Nature* **2001**, 414, 332-337.
- [9] Zhang, T.; Low, J.; Koh, K.; Yu, J.; Asefa, T. Mesoporous TiO₂ comprising small, highly crystalline nanoparticles for efficient CO₂ reduction by H₂O. *ACS Sustainable Chem. Eng.* **2018**, 6, 531-540.
- [10] Fujishima, A.; Honda, K. Electrochemical photolysis of water at semiconductor electrode. *Nature* **1972**, 238, 37.
- [11] Hoffmann, M. R.; Martin, S. T.; Choi, W. Bahnemann, D. W. Environmental Applications of Semiconductor Photocatalysis. *Chem. Rev.* **1995**, 95, 69.

- [12] Jung, K. Y.; Park, S.; Son K. I. Linear relationship between the crystallite size and the photoactivity of non-porous titanium ranging from nanometer to micrometer size. *Appl. Catal., A* **2002**, 84, 181-189.
- [13] Yue, W.; Randorn, C.; Attidekou, P. S.; Su, Z.; Irvine, J. T. S.; Zhou, W. Syntheses, Li insertion, and photoactivity of mesoporous crystalline TiO₂. *Adv. Funct. Mater.* **2009**, 19, 2826–2833.
- [14] Jiang, X.; Herricks, T.; Xia, Y. Monodispersed spherical colloids of titania: synthesis, characterization, and crystallization. *Adv. Mater.* **2003**, 15, 1205–1209.
- [15] Kominami, H.; Jun, I.; K.; Shin, Y.; M, Solvothermal syntheses of semiconductor photocatalysts of ultra-high activities. *J. Catal. Today.* **2003**, 84, 181-189.
- [16] Choi, W.; Termin, A.; Hoffmann, M. R.; The role of metal ion dopants in quantum sized TiO₂: correlation between photoreactivity and charge carried recombination Dynamics. *J. Phys. Chem.* **1994**, 98, 13669-13769.
- [17] Zhang, T.; Low, J.; Huang, X.; Al-Sharab, J. F., Yu, J.; Asefa, Y. Copper decorated microsized nanoporous titanium dioxide photocatalysts for carbon dioxide reduction by water. *ChemCatChem* **2017**, 9, 3054-3062.
- [18] Zhang M.; An, T.; Hu X. Preparation and photocatalytic properties of a nanometer ZnO-SnO₂ coupled oxide. *J. Appl. Catal., A.* **2001**, 165, 265-273
- [19] Zhang, H.; Banfield, J. F. Thermodynamic analysis of phase stability of nanocrystalline titania. *J. Mater. Chem.* **1998**, 8, 2073–2076.
- [20] Carraway, E. R.; Hoffmann A. J.; Hoffmann, M. R. Photocatalytic production of H₂O₂ and organic peroxides on quantum-sized semiconductor colloids. *Environ. Sci. Technol.* **1994**, 28, 776-785.
- [21] Cohen, M. L.; Calculation of bulk moduli of diamond and zine-blende solids. *J. Phys. Rev. B.*, **1985**, 32, 7988-7991.

- [22] Liu, A. Y.; Cohen, M. L. Prediction of new low compressibility Solids. *Science*. **1989**, 245, 841-842.
- [23] Li, Q.; Xie, R.; Li, Y. Mintz, E. A.; Shang, J. K. Enhanced visible-light-induced photocatalytic disinfection of E-coli by carbon-sensitized nitrogen-doped titanium oxide. *J. Environ. Sci. Technol.* **2007**, 41, 5050-5056.
- [24] Teter, D. M.; Hemley, R. J. Low-compressibility Carbon Nitride. *Science* **1996**, 271, 53-55.
- [25] Cao, S. W.; Low, J. X.; Jaroniec M. Polymeric photocatalysts based on graphitic carbon nitride. *Adv. Mater.* **2015**, 27, 2150-2176
- [26] Kroke, E.; Schwarz, M.; Horath B. E.; Kroll, P.; Noll, B.; Norman, A. D. Tri-s-triazine derivatives. Part I. From trichloro-tri-s-triazine to graphitic C₃N₄ structures. *J. New J. Chem.* **2002**, 26, 508-512.
- [27] Wang, X.; Blechert, S.; Antonietti, M. Polymeric graphitic carbon nitride for heterogeneous photocatalysis. *J. ACS. Catal.* **2012**, 2, 1596-1606.
- [28] Yan, S. C.; Li, Z. S.; Zou, Z. G. Photodegradation performance of g-C₃N₄ fabricated by directly heating melamine. *J. Langmuir*, **2009**, 25, 10397-10401.
- [29] Wang, X. C.; Maeda, K.; Chen, X. F.; Takanebe, K.; Domen, K.; Hou, Y. D.; Fu, X. Z.; Antonietti, M. Polymer semiconductors for artificial photosynthesis: hydrogen evolution by mesoporous graphitic carbon nitride with visible light. *J. Am. Chem. Soc.* **2009**, 131, 1680-1681.
- [30] Wang, X. C. Chen, X. F.; Thomas, A.; Fu, X. Z.; Antonietti, M. Metal-containing carbon nitride compounds: A new functional organic-metal hybrid material. *J. Adv. Meter.* **2009**, 21, 1609-1612.

- [31] Jourshabani, M.; Shariatinia, Z.; Badiei, A. Sulfur-doped mesoporous carbon nitride decorated with Cu particles for efficient photocatalytic degradation under visible-light irradiation. *J. Phys. Chem. C* **2017**, 121, 19239-19253
- [32] Zhang, J.; Sun, J.; Maeda, K.; Domen, K.; Liu, P.; Antonietti, M.; Fu, X.; Wang, X. Sulfur-mediated synthesis of carbon nitride: band-gap engineering and improved functions for photocatalysis. *Energy Environ. Sci.* **2011**, 4, 675–678.
- [33] Thomas, A.; Fischer, A.; Goettmann, F.; Antonietti, M.; Müller, J.-O.; Schlögl, R.; Carlsson, J. M. Graphitic carbon nitride materials: variation of structure and morphology and their use as metal-free catalysts. *J. Mater. Chem.* **2008**, 18, 4893–4908.
- [34] Jourshabani, M.; Badiei, A.; Lashgari, N.; Ziarani, G. M. Highly selective production of phenol from benzene over mesoporous silica-supported chromium catalyst: role of response surface methodology in optimization of operating variables. *Chin. J. Catal.* **2015**, 36, 2020–2029.
- [35] Hu, S.; Ma, L.; You, J.; Li, F.; Fan, Z.; Lu, G.; Liu, D.; Gui, J. Enhanced visible light photocatalytic performance of g-C₃N₄ photocatalysts Co-Doped with iron and phosphorus. *Appl. Surf. Sci.* **2014**, 311, 164–171.
- [36] Zhang, S.; Li, J.; Zeng, M.; Zhao, G.; Xu, J.; Hu, W.; Wang, X. In Situ synthesis of water-soluble magnetic graphitic carbon nitride photocatalyst and its synergistic catalytic performance. *ACS Appl. Mater. Interfaces* **2013**, 5, 12735–12743.
- [37] Cheng, N.; Tian, J.; Liu, Q.; Ge, C.; Qusti, A. H.; Asiri, A. M.; Al-Youbi, A. O.; Sun, X. Au-nanoparticle-loaded graphitic carbon nitride nanosheets:

- green photocatalytic synthesis and application toward the degradation of organic pollutants. *ACS Appl. Mater. Interfaces* **2013**, 5, 6815–6819.
- [38] Souza, I. P. A. F.; Pezoti, O.; Bedin, K. C.; Cazetta, B. A.; Melo, S. A. R.; Souza, L. S.; Silva, M. C.; Almeida, V. C. Chemometric study of thermal treatment effect on P25 photoactivity for degradation of tartrazine yellow dye. *Ceramics International* **2018**, 4, 16.
- [39] Gupta, V. K.; Jain, R.; Nayak, A.; Agarwal, S.; Shrivastava, M. Removal of the hazardous dye—Tartrazine by photodegradation on titanium dioxide surface. *Material Science and Engineering C* **2011**, 31, 1062-1067.
- [40] Walton, K.; Walker, R.; Sandt, J.J.M.; Castell, J.V. The application of in vitro data in the derivation of the acceptable daily intake of food additives. *Food Chem. Toxicol.* **1999**, 37, 1175–1197.
- [41] Sweeney, A.E.; Chipman, J.K.; Forsythe, S.J. Evidence for direct-acting oxidative genotoxicity by reduction products of azo dyes. *Environ. Health Perspect.* **1994**, 102, 119–122.
- [42] Siraki, A.G.; Chan, T.S.; Galati, G.; Teng, S.; O'Brien, P.J. N-oxidation of aromatic amines by intracellular oxidases. *Drug Metab. Rev.* **2002**, 34, 549–564.
- [43] Ezeuko, V.C.; Nwokocha, C.R.; Mounmbegna, P.E.; Nriagu, C.C. Effect of *Zingiber officinale* on liver function of mercuric chloride induced hepatotoxicity in adult male Wistar rats. *Electron. J. Biomed.* **2007**, 3, 40–45
- [44] Sasaki, Y.F.; Kawaguchi, S.; Kamaya, A.; Ohshita, M.; Kabasawa, K.; Iwama, K.; Taniguchi, K.; Tsuda, S. The comet assay with 8 mouse organs:

results with 39 currently used food additives. *Mutat. Res.* **2002**, 519 (1–2), 103–119.

[45]He, J.; Giusti, M. M. Anthocyanins: Natural colorants with health-

promoting properties. *Annu. Rev. Food Sci. Technol.* **2010**, 1, 163-187

[46]Zhang, T., Huang, X.; Asefa, Y. Nanostructured polymers with high surface

area using inorganic templates for the efficient extraction of anionic dyes

from solutions. *Chem. Commun.* **2015**, 51, 16135-16138.

[47]Robert L. Hirsch, Ph.D. Senior Energy Program Advisor, Peaking of World

Oil Production, How Do We Mitigate the Problem *SAIC July, 2015.*